

Salt stress activates the CDK8-AHL10-SUVH2/9 module to dynamically regulate salt tolerance in *Arabidopsis*

Received: 12 May 2024

Accepted: 4 March 2025

Published online: 12 March 2025



Pengcheng Guo^{1,4}, Leelyn Chong^{1,4}, Zhixin Jiao¹, Rui Xu¹, Qingfeng Niu² & Yingfang Zhu^{1,3} ✉

Salt stress has devastating effects on agriculture, yet the key regulators modulating the transcriptional dynamics of salt-responsive genes remain largely elusive in plants. Here, we discover that salt stress substantially induces the kinase activity of Mediator cyclin-dependent kinase 8 (CDK8), which is essential for its positive role in regulating salt tolerance. CDK8 is identified to phosphorylate AT-hook motif nuclear-localized protein 10 (AHL10) at serine 314, leading to its degradation under salt stress. Consistently, AHL10 is found to negatively regulate salt tolerance. Transcriptome analysis further indicates that CDK8 regulates over 20% of salt-responsive genes, half of which are co-regulated by AHL10. Moreover, AHL10 is revealed to recruit SU(VAR)3-9 homologs (SUVH2/9) to AT-rich DNA sequences in the nuclear matrix-attachment regions (MARs) of salt-responsive gene promoters, facilitating H3K9me2 deposition and repressing salt-responsive genes. Our study thereby has identified the CDK8-AHL10-SUVH2/9 module as a key molecular switch controlling transcriptional dynamics in response to salt stress.

Soil salinization poses a number of harmful effects to plants. High concentrations of sodium (Na⁺) and chloride (Cl⁻) ions can cause leaf yellowing, delayed flowering, height reduction, and even death to plants¹. To cope with salt stress, plants have evolved various adaptive mechanisms^{2,3}. One of these mechanisms includes the conserved salt overly sensitive (SOS) signaling pathway comprising SOS3, SOS2, and SOS1 proteins. Aside from activating the SOS pathway to maintain ion homeostasis at the cellular level, plants also utilize the SOS proteins to reorganize cytoskeleton and root architecture in response to salt stress^{4–11}. Another salt stress response mechanism involves the LRX3/4/5-RALF22/23-FER module, which can integrate plant hormones such as jasmonic acid (JA), salicylic acid (SA), and abscisic acid (ABA) to modulate plant growth and salt tolerance^{12–14}. Transcription factors (TFs) that are known to be highly inducible by salt stress include the dehydration-responsive element binding protein 2 (*DREB2A*),

Arabidopsis NAC domain-containing protein 40 (*ANAC040*) and WRKY DNA-binding protein 75 (*WRKY75*)^{15–17}. These elements work in concert to turn on a myriad of stress-responsive genes to help the plant adapt and survive in high-salt environments. Despite these knowledge, there remains a significant gap in our understanding of the main regulatory mechanisms that govern the salt stress response in plants.

One critical aspect of gene regulation is the Mediator complex. The Mediator is a large, multi-subunit protein complex that regulates transcription at the level of RNA Polymerase II (RNA Pol II) assembly^{18–20}. This complex consists of 25–30 subunits, which are divided into distinct modules including the head, middle, tail, and cyclin-dependent kinase 8 (CDK8) modules. The Mediator complex acts as an essential bridge, transducing regulatory signals from TFs to the transcriptional machinery to induce or repress target gene expression²¹. A particularly noteworthy subunit of the Mediator

¹The Zhongzhou Laboratory for Integrative Biology, State Key Laboratory of Crop Stress Adaptation and Improvement, School of Life Sciences, Henan University, Kaifeng 475004, China. ²National Engineering Laboratory of Crop Stress Resistance Breeding, School of Life Sciences, Anhui Agricultural University, Hefei 230036, China. ³Sanya Institute of Henan University, Sanya, Hainan 572025, China. ⁴These authors contributed equally: Pengcheng Guo, Leelyn Chong. ✉e-mail: zhuyf@henu.edu.cn

complex is CDK8, which has been shown to play positive roles in plant immunity, ABA signaling and drought responses in plants. Through interacting with diverse TFs, CDK8 is able to modulate stress-responsive genes^{22–26}. However, the specific substrates of CDK8 and the molecular mechanisms by which it regulates the transcription of stress-responsive genes remain elusive.

One key player in this process is the AT-Hook Motif Nuclear Localized (AHL) family of TFs. These proteins contain two characteristic AT-HOOK motifs that allow them to bind to AT-rich regions of DNA and a Plant and Prokaryote Conserved (PPC) domain²⁷. Several members of the AHL family have been reported to play important roles in organ development, flowering, defense responses, and maintaining the balance between stress adaptation and growth^{28–31}. Importantly, AHL proteins are thought to be localized within the nuclear matrix, concentrated at the boundaries between euchromatin and heterochromatin regions. In this position, they are poised to bind to matrix attachment regions (MARs), which are genomic sequences abundant in AT motifs that are typically associated with transcriptional repression³². Through these interactions, AHLs could potentially regulate chromatin structure, histone modifications, and the transcription of stress-responsive genes^{33,34}. Recent studies have shown that stress signaling pathways can regulate the activity of AHL proteins to modulate the balance between stress adaptation and growth in plants³⁵. In particular, AHL10 has emerged as a key player, whose activity is regulated through phosphorylation, ultimately affecting the chromatin association of the regulatory protein RRP6L³⁶. However, the precise mechanisms governing AHL10 activity remain to be investigated. The upstream kinases responsible for phosphorylating and regulating AHL10 protein stability, such as the potentially important CDK8 kinase, need to be elucidated.

In the context of histone modifications, SUV(VAR)3-9 homologs (SUVHs) in Arabidopsis are a family of 10 proteins that play a key role in catalyzing the methylation of histone H3 at lysine 9 (H3K9me2)³⁷. Three members of this family, SUVH4, SUVH5, and SUVH6 (SUVH4/5/6), have been reported to directly catalyze the demethylation of H3K9 and enhance the methylation of DNA at CHG sites³⁸. Meanwhile, two other SUVH proteins, SUVH2 and SUVH9 (SUVH2/9), lack intrinsic histone methyltransferase activity but still can repress gene expression through a process known as RNA-directed DNA methylation (RdDM)^{39,40}. Interestingly, recent studies have shown that SUVH2/9 can recruit the SUVH4/5/6 proteins, thereby affecting H3K9me2 levels⁴¹. Furthermore, the significant reduction of H3K9me2 levels observed in *svh2/9* double mutants highlights the importance of these interactions^{42,43}. However, the specific recruitment factors that facilitate the actions of SUVH2/9 remain poorly characterized, presenting a compelling frontier for further exploration in the field of epigenetic regulation.

In our study, we uncovered a dynamic molecular switch that plays a critical role in integrating multiple layers of regulation, including epigenetic mechanisms for plants responding to salt stress. Our findings indicated that salt stress activates the kinase activity of Mediator CDK8, which directly interacts with AHL10 and phosphorylates it at serine 314 (Ser314). This phosphorylation event promotes the degradation of AHL10, thus facilitating salt stress tolerance in plants. Furthermore, our work highlights the dual role of AHL10 in transcription under salt stress conditions. We found that AHL10 can mediate transcriptional repression by directly binding to MARs with AT-rich sequences present in the salt-responsive gene promoters. This binding is significant as it allows AHL10 to regulate H3K9me2 levels through the recruitment of epigenetic regulators SUVH2/9. Thus, AHL10 serves as a crucial player in the transcriptional repression of salt stress-responsive genes. The intricate mechanism that we identified exemplifies that plants can integrate multiple regulatory processes, including kinase-mediated phosphorylation, transcriptional modulation, and epigenetic control, to mount a sophisticated response to stresses imposed by high salinity.

Results

CDK8 positively regulates salt tolerance

CDK8 has been reported to play an important role in plant development, immunity and drought stress responses^{22,24}. Its role in salt stress response, however, remains unclear. To explore this, we first examined the phenotypic effects arising from loss-of-function mutations in *CDK8*. Two distinct *CDK8* mutant lines (*cdk8-1* and *cdk8-2*) were subjected to salt treatment and compared against a wild-type (WT) control. The results revealed a striking hypersensitivity within the *CDK8* mutant lines. Both mutant lines exhibited significantly more pronounced phenotypic changes under salt stress compared to the WT. During the seed germination stage, the percentage of green cotyledon was significantly lower when compared to the WT (Supplementary Fig. 1a, b). In addition, remarkably shorter primary roots were noted in the mutants (Fig. 1a, b, Supplementary Fig. 1c). On the other hand, *CDK8* over-expression lines (*CDK8-YFP #6* and *CDK8-YFP #11*) had higher green cotyledon percentages (Supplementary Fig. 1a, b) and longer primary roots compared to the WT (Fig. 1a, b, Supplementary Fig. 1c), indicating that CDK8 may play a role in salt stress response. To further investigate the implications of CDK8 expression on plant survival under salinity conditions, both WT and over-expression lines were subjected to salt stress in soil. Approximately 70% of the WT plants, along with all *CDK8* over-expression transgenic plants, managed to survive the salt treatment. In contrast, the majority of the *cdk8* mutants did not withstand the stress (Fig. 1c, d), suggesting that *CDK8* is a positive regulator of salt tolerance.

Salt stress enhances the kinase activity of CDK8

We next investigated how salt stress affects CDK8 at the transcription levels. Quantitative reverse transcription PCR (RT-qPCR) analyses indicated a slight decrease in *CDK8* expression at early time points. However, a notable increase was observed after 3 h of NaCl treatment (Supplementary Fig. 2a). Consistently, a significant increase in the GUS activity driven by the CDK8 promoter was observed in *CDK8pro:GUS* transgenic seedlings after NaCl treatment (Supplementary Fig. 2b). The effect of salt stress on CDK8 protein abundance was then evaluated. While the overall levels of the CDK8 protein remained relatively stable following salt treatment, a significant change was observed in its kinase activity (Fig. 1e). This indicates that salt stress may not directly influence the expression of the CDK8 protein, but it could potentially modulate its activity. As shown in Fig. 1f, CDK8 exhibited relatively weak kinase activity under normal conditions. However, there was a significant enhancement in its activity after salt treatment, highlighting the involvement of CDK8 in the adaptive mechanisms of Arabidopsis to salt stress. To check if the kinase activity of CDK8 is required for salt tolerance, we conducted a comparative analysis of salt phenotypes among *CDK8-MYC* and *CDK8-KD-MYC* (KD: kinase-dead) transgenic lines in a *cdk8* background²⁵. *CDK8-MYC* was found to successfully rescue the salt hypersensitivity observed in *cdk8* mutants. This was evidenced by measurements of the primary root length and the percentages of green cotyledon. We noted that these data in the *CDK8-MYC/cdk8-1* line were similar to those of the WT grown in a salt medium (Fig. 1g, h, Supplementary Fig. 3a, b, c). However, the expression of the kinase-dead version of *CDK8* failed to mitigate the salt sensitivity of the *cdk8* mutant, suggesting the necessity of the CDK8's kinase activity in conferring salt tolerance in Arabidopsis.

CDK8 interacts with and phosphorylates AHL10 under salt stress conditions

To further elucidate the regulatory role of CDK8 in the salt stress response of Arabidopsis, we utilized a phosphoproteomics technology that we recently optimized^{44,45} and identified putative substrates of CDK8. While several CDK8 substrates have already been characterized in eukaryotic systems such as human and yeast cells, only a handful of CDK8 substrates have been identified in plant systems^{46,47}. This gap in

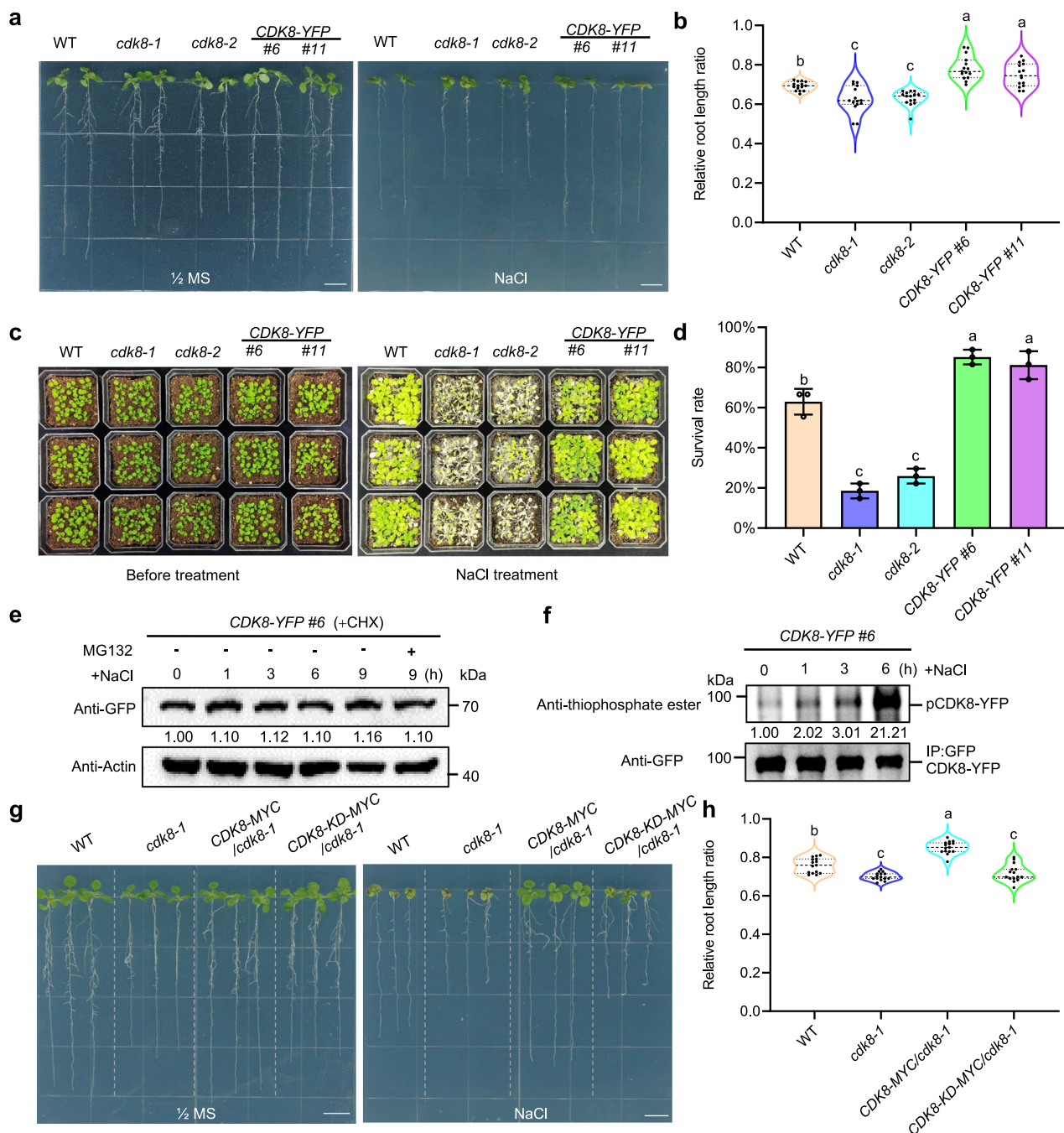


Fig. 1 | *CDK8* positively regulates salt tolerance. **a** The root growth of the WT, *cdk8-1*, *cdk8-2* and *CDK8-YFP* transgenic seedlings grown on $\frac{1}{2}$ MS plates with or without 0.1 M NaCl. **b** Relative primary root length ratio of the WT, *cdk8-1*, *cdk8-2* and *CDK8-YFP* transgenic seedlings in (a). Values are means \pm SD ($n = 15$). Different letters indicate statistically significant differences by one-way ANOVA (Tukey's multiple comparisons test, $P < 0.01$). **c** The salt tolerance phenotype of WT, *cdk8-1*, *cdk8-2* and *CDK8-YFP* transgenic seedlings grown in soil. **d** Survival rate corresponding to (c). Values are means \pm SD from three biological replications. Different letters indicate statistically significant differences by one-way ANOVA (Tukey's multiple comparisons test, $P < 0.01$). **e** Immunoblots showing the CDK8 protein abundance under salt stress. Total proteins were extracted from *CDK8-YFP*

transgenic plants treated with 0.2 M NaCl for the indicated time. Actin was used as a control. **f** Analysis of CDK8 kinase activity in response to salt treatment. Autophosphorylation of CDK8 was examined using an anti-thiophosphate ester antibody. The intensity of each band was measured using ImageJ software. **g** The root growth of the WT, *cdk8-1*, *CDK8-MYC/cdk8-1* and *CDK8-KD-MYC/cdk8-1* transgenic seedlings grown on $\frac{1}{2}$ MS plates with or without 0.1 M NaCl ($n = 15$). **h** Relative primary root length ratio of the WT, *cdk8-1*, *CDK8-MYC/cdk8-1* and *CDK8-KD-MYC/cdk8-1* transgenic seedlings in (g). Values are means \pm SD ($n = 15$). Different letters indicate statistically significant differences by one-way ANOVA (Tukey's multiple comparisons test, $P < 0.01$).

knowledge highlights the need for further research. In our investigation, two independent replicates of the experiment yielded a total of 97 overlapping putative substrates of CDK8 (Supplementary Data 1). We then focused on validating substrates of interest through the yeast

two-hybrid (Y2H) system. Among the candidates examined, we chose to investigate AHL10. AHL proteins have been demonstrated to play vital roles in regulating plant growth and development³¹. Among these, AHL10, which belongs to clade B of the AT-hook TF family has been

identified as a crucial member. Through our Y2H assays, we observed that the full-length AHL10 as well as its C-terminal region 159 to 351 amino acids (aa), exhibited a physical interaction with CDK8. In contrast, the N-terminal portion of AHL10 (1–158 aa) did not demonstrate such an interaction, indicating that the C-terminal domain is crucial for this association (Fig. 2a). These results thereby suggested that AHL10 could be a significant target of CDK8. Our subcellular localization assays showed that AHL10 is localized within the nucleus (Supplementary Fig. 4).

To further validate the protein interaction between CDK8 and AHL10, we employed bimolecular fluorescence complementation (BiFC) assays and demonstrated that CDK8 and AHL10 interact specifically within the nucleus, as indicated by the reconstitution of fluorescent signals in the nuclei of co-expressing cells (Fig. 2b). Their interactions were also assessed by co-immunoprecipitation (Co-IP) assays with stable transgenic plants *CDK8-MYC*, *AHL10-GFP*, and *AHL10-GFP/CDK8-MYC*. The Co-IP results indicated successful precipitation of CDK8-MYC by AHL10-GFP (Fig. 2c). A luciferase complementation imaging (LCI) assay was further used to complement our findings. We observed strong LUC signals when *N. benthamiana* leaves were co-infiltrated with CDK8-nLUC and cLUC-AHL10, confirming the existence of a functional interaction between these two proteins. This finding was further corroborated by the positive control, where we observed robust LUC activity with the combination of CDK8-nLUC and cLUC-Cyclin C (CYCC). In contrast, the negative controls failed to show any detectable LUC activity, reinforcing the specificity of the interactions we identified. The immunoblot analysis provided additional validation of the protein expression of each fusion protein observed in the LCI assays (Fig. 2d).

Following our confirmation of the interaction between the proteins CDK8 and AHL10, we proceeded to investigate how salt stress influences their interaction. To achieve this, we performed Co-IP assays with stable transgenic plants that co-expressed *CDK8-MYC* and *AHL10-GFP* and subjected to conditions with or without salt treatment. Our results revealed that salt stress enhances the interaction between CDK8-MYC and AHL10-GFP (Fig. 2e). This enhancement suggested that salt stress may play an important role in the functional relationship between CDK8 and AHL10, potentially influencing downstream signaling pathways and stress response mechanisms.

AHL10 negatively regulates salt tolerance

In light of the physical interaction observed between AHL10 and CDK8 under salt stress conditions, we next wanted to confirm whether AHL10 is involved in the salt stress response. We first isolated the *ahl10* mutants in which the T-DNA inserted into the fifth exon of the *AHL10* gene, leading to a loss-of-function phenotype *ahl10* (SALK_010945). The homozygosity of the *ahl10* mutants was verified by PCR (Supplementary Fig. 5a). In addition, we generated two independent lines of transgenic plants with overexpressed *AHL10-GFP* (*AHL10-GFP* #48 and #61) for comparisons. Immunoblot analysis indicated an expression of the AHL10-GFP fusion protein in the *AHL10-GFP* #48 and *AHL10-GFP* #61 transgenic seedlings but not in the WT and *ahl10* mutant seedlings (Supplementary Fig. 5b). RT-qPCR results further showed that *AHL10* expression was significantly up-regulated in *AHL10-GFP* #48 and *AHL10-GFP* #61 transgenic plants but barely discernible in *ahl10* mutants, confirming successful integration and expression of the transgene (Supplementary Fig. 5c).

We subsequently examined the phenotypes of WT, *ahl10* and *AHL10-GFP* transgenic plants at the seed germination and young seedling stages under salt stress. Compared to the WT, *ahl10* mutants exhibited enhanced salt tolerance, resulting in higher cotyledon greening rate (Supplementary Fig. 6a, b) and longer primary root length (Fig. 3a, b, Supplementary Fig. 7a). In contrast, *AHL10-GFP* transgenic plants were hypersensitive to salt treatment, showing reduced cotyledon greening rate (Supplementary Fig. 6a, b) and

shorter primary root length (Fig. 3a, b, Supplementary Fig. 7a). Moreover, we tested their salt tolerance in soil conditions. As illustrated in Fig. 3c, d, more than 80% of the *ahl10* mutant plants survived after salt treatment in soil, while only less than 60% of the WT and 20% of the *AHL10-GFP* transgenic plants survived. To further validate these findings, we utilized CRISPR-Cas9 to create two new *ahl10* mutant lines (*ahl10-cri* #1 and #7) with 1-bp deletion and 1-bp insertion, respectively (Fig. 3e). After transferring them to NaCl plates, the new *ahl10* mutant lines showed enhanced salt tolerance with longer root length in comparison to WT (Fig. 3f, g, Supplementary Fig. 7b), which further indicated that *AHL10* has a negative role in salt stress response.

CDK8 specifically phosphorylates the Ser314 of AHL10

Our phosphoproteomics data identified that the serine (Ser) residues 313, 314 and 317 within the AHL10 are potential phosphorylation targets for CDK8 (Fig. 4a). To determine the phosphorylation sites influenced by CDK8 on AHL10, we performed an in vitro kinase reaction assay. Following this, we employed mass spectrometry analysis and our results showed that CDK8 phosphorylates serine 313, 314 and 317 of AHL10 (Supplementary Fig. 8). To determine the specific serine site in AHL10 that is phosphorylated by CDK8, we purified recombinant proteins MBP-CDK8 and various His-tagged AHL10 variants (His-AHL10^{S313A}, His-AHL10^{S314A}, His-AHL10^{S317A}, His-AHL10^{S314A/S317A}, and His-AHL10^{S313A/S314A/S317A}). These variants featured specific mutations where serine residues were substituted with alanine. Our in vitro phosphorylation assays yielded important insights, revealing that CDK8 can phosphorylate AHL10, AHL10^{S313A}, AHL10^{S317A} but not AHL10^{S314A}, AHL10^{S314A/S317A}, and AHL10^{S313A/S314A/S317A}, suggesting that Ser314 is the critical residue in AHL10 for CDK8-mediated phosphorylation (Fig. 4b).

Salt stress-induced phosphorylation and degradation of AHL10 requires CDK8

Next, we wanted to investigate whether salt stress could increase the CDK8-mediated AHL10 phosphorylation because it was demonstrated to enhance the kinase activity of CDK8. To test this, we generated *AHL10-GFP* transgenic lines in both WT and *cdk8-1* mutant backgrounds. We then compared the phosphorylation status of AHL10 in vivo, utilizing phos-tag gel shift assays to assess the impact of salt treatment. Our results showed that the transgenic lines in the WT background exhibited distinct phosphorylation migration bands after NaCl treatment, suggesting an increase in the phosphorylated form of AHL10 in response to salt stress. However, the transgenic lines in *cdk8* background displayed no discernible migration bands (Fig. 4c), indicating that salt stress-induced phosphorylation of AHL10 is largely dependent on the kinase activity of CDK8.

We then examined the effect of salt stress on the transcription and protein levels of AHL10. Our RT-qPCR results showed that the transcription of *AHL10* was slightly repressed by salt treatment (Supplementary Fig. 9a). Conversely, we noted a significant decrease in the abundance of AHL10 protein after salt treatment (Supplementary Fig. 9b, c). To further understand this phenomenon, we applied the protein biosynthesis inhibitor Cycloheximide (CHX) to check for protein stability. We found that salt stress can induce the degradation of AHL10 and its degradation was inhibited when treated with the 26S proteasome inhibitor MG132 (Supplementary Fig. 9d), suggesting a proteasome-dependent pathway for AHL10 turnover under salt stress conditions. In addition, we also assessed the protein stability of AHL10 in response to mannitol treatment. Interestingly, mannitol treatment did not significantly affect the protein levels of AHL10 (Supplementary Fig. 9e, f), implying that the degradation of AHL10 may be a specific response to salt stress.

Furthermore, we investigated the biological functions of salt-stress induced AHL10 phosphorylation. We generated transgenic plants *AHL10-GFP/ahl10*, *AHL10^{S314A}-GFP/ahl10*, and *AHL10^{S314D}-GFP/ahl10* and we used immunoblot assays to confirm the expression of those fusion

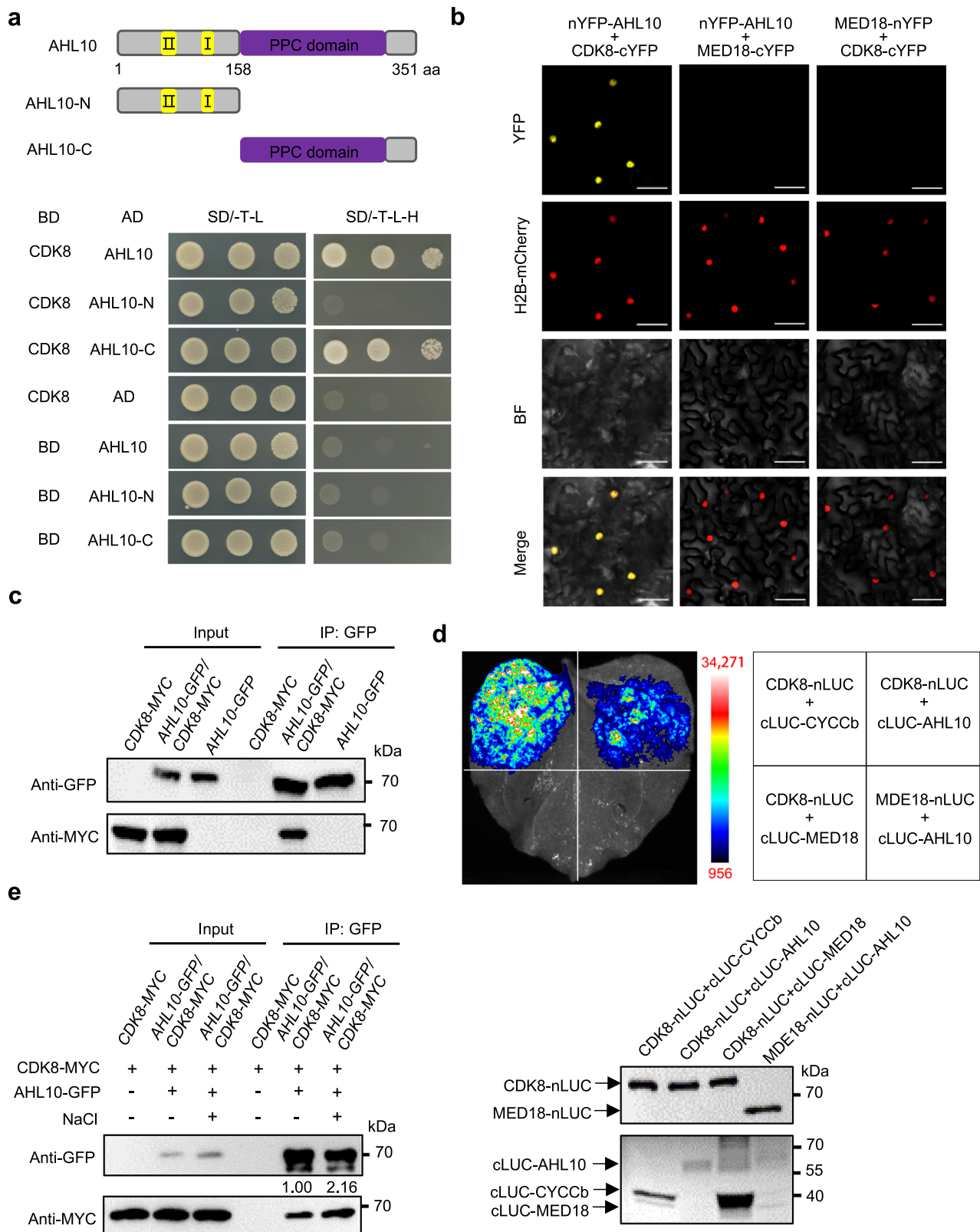


Fig. 2 | CDK8 physically interacts with AHL10. **a** Y2H assays showing the physical interaction of CDK8 with AHL10. **b** CDK8 interacts with AHL10 in BiFC assays. MED18 was used as a negative control. Scale bar = 50 μ m. **c** Co-IP assays confirming the CDK8-AHL10 interaction in vivo. Transgenes expressing CDK8-MYC and AHL10-GFP alone were the negative controls. **d** LCI assays showing the interaction between CDK8 and AHL10 in tobacco leaves. MED18 was used as a negative control. CYCCb

was used as a positive control. Immunoblot confirmed the protein expression of nLUC and cLUC fusions, as determined with anti-luciferase and anti-cLUC antibodies. **e** Co-IP assays confirmed that salt stress resulted in enhanced CDK8-AHL10 interactions in vivo. Transgenes expressing CDK8-MYC alone were negative controls. Two independent experiments were conducted with similar results.

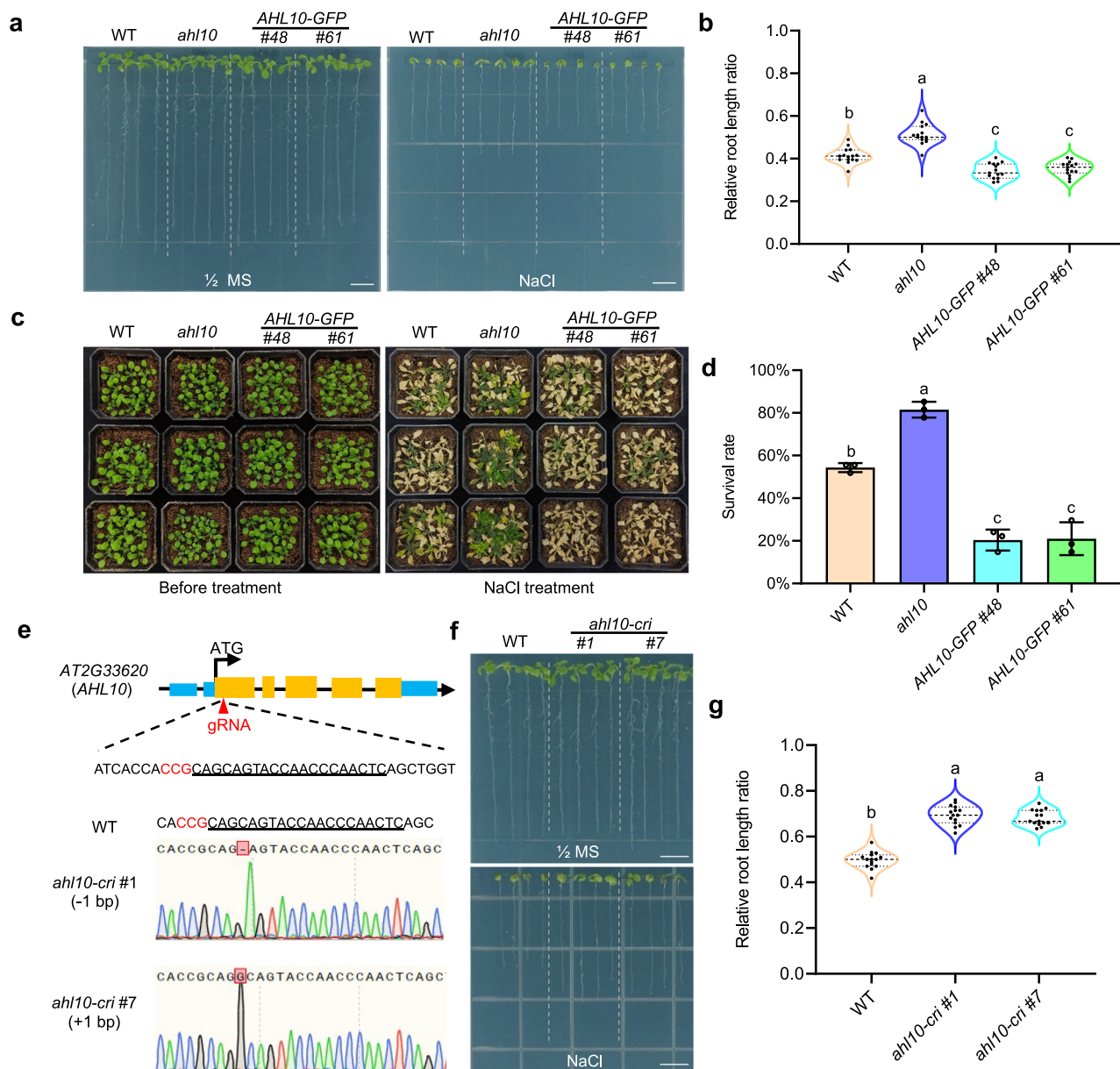


Fig. 3 | *AHL10* negatively regulates salt tolerance. **a** The root growth of the WT, *ahl10* and *AHL10-GFP* transgenic seedlings (#48 and #61) grown on $\frac{1}{2}$ MS plates with or without 0.1 M NaCl. **b** Relative primary root length ratio of the WT, *ahl10* and *AHL10-GFP* transgenic seedlings in (a). Values are means \pm SD ($n = 15$). Different letters indicate statistically significant differences by one-way ANOVA (Tukey's multiple comparisons test, $P < 0.01$). **c** The salt tolerance phenotype of WT, *ahl10* and *AHL10-GFP* transgenic seedlings grown in soil. **d** Survival rate corresponding to (c). Values are means \pm SD from three independent replicates. Different letters

indicate statistically significant differences by one-way ANOVA (Tukey's multiple comparisons test, $P < 0.01$). **e** Schematic diagram of *AHL10*-CRISPR types. **f** The root growth of the WT, *ahl10-cri* #1 and *ahl10-cri* #7 transgenic plants on $\frac{1}{2}$ MS plates with or without 0.1 M NaCl. **g** Relative primary root length ratio of WT, *ahl10-cri* #1 and *ahl10-cri* #7 transgenic seedlings in (f). Values are means \pm SD ($n = 15$). Different letters indicate statistically significant differences by one-way ANOVA (Tukey's multiple comparisons test, $P < 0.01$).

proteins (Supplementary Fig. 10). We subsequently demonstrated that *AHL10* protein was degraded in the *AHL10-GFP/ahl10* transgenic seedlings under salt treatment as opposed to water treatment (Fig. 4d, h). In contrast, *AHL10^{S314A}-GFP/ahl10* transgenic plants showed disruptions in this process (Fig. 4e, h). Interestingly, the *AHL10^{S314D}-GFP/ahl10* transgenic plants showed an even faster rate of protein degradation rate (Fig. 4f, h), implying that Ser314 phosphorylation is vital for the protein stability of *AHL10* in response to salt stress.

To further study whether *CDK8* contributes to the salt stress-induced protein degradation of *AHL10*, we generated *AHL10-GFP/cdk8* transgenic plants (Supplementary Fig. 10) and conducted protein degradation experiments. We found that salt-induced degradation of

AHL10 protein was inhibited in the presence of *CDK8* mutations (Fig. 4g, h). This implies that salt-induced *AHL10* protein degradation is partially dependent on *CDK8*.

The genetic relationship between *CDK8* and *AHL10* in the salt stress response

To investigate the genetic relationship between *CDK8* and *AHL10*, we generated a *cdk8-1 ahl10* double mutant. The *cdk8-1 ahl10* double mutants were verified to be homozygous by PCR (Supplementary Fig. 11a). Subjecting these mutants to salt treatment, we observed a marked reduction in the cotyledon greening rates in the double mutant when compared to both the WT and *ahl10* (Supplementary

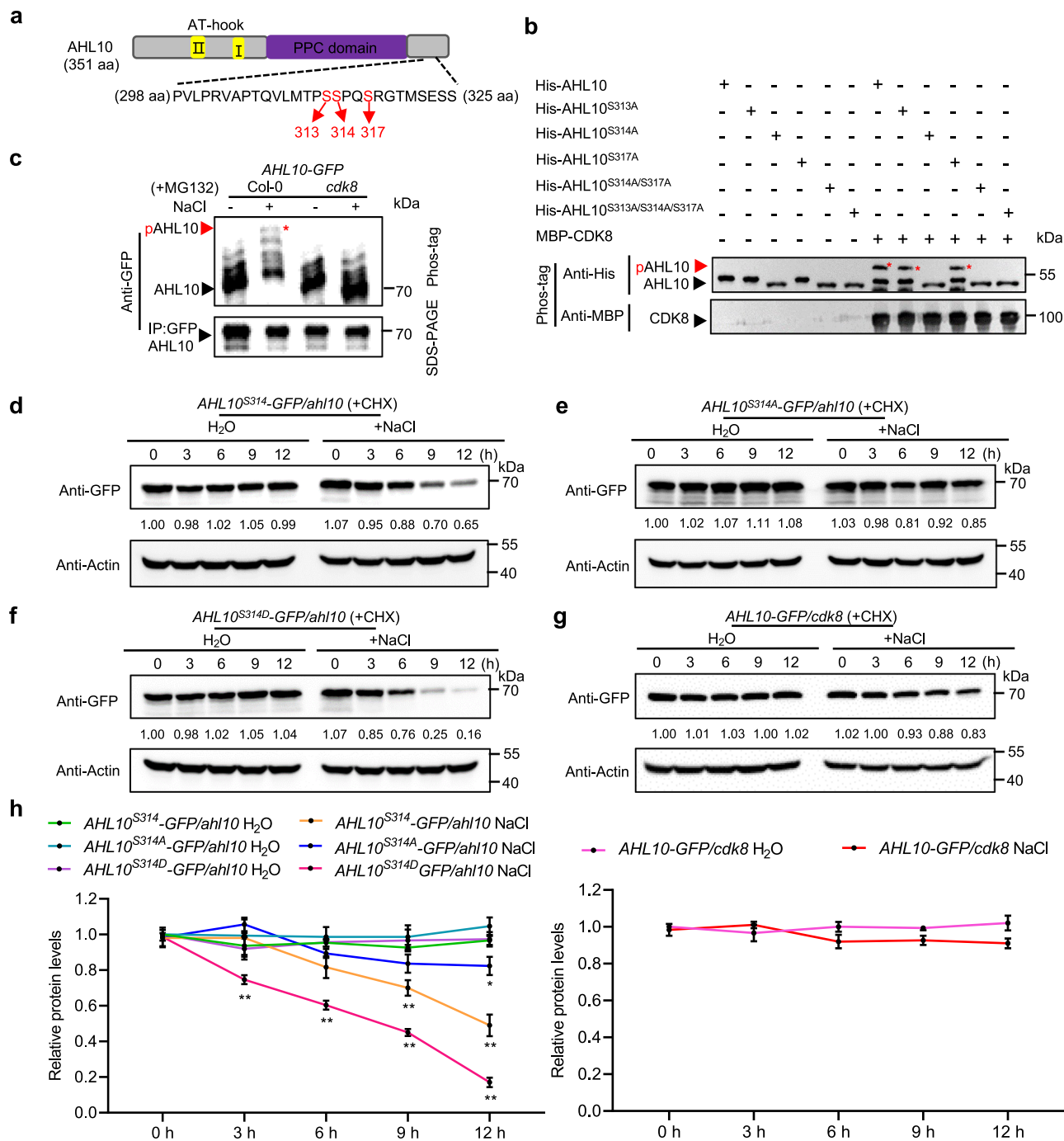


Fig. 4 | CDK8 phosphorylates the Ser314 of AHL10 and promotes its protein degradation. **a** The phospho-sites of AHL10 identified from phosphoproteomics analysis. **b** Phos-tag mobility shift assays validated the AHL10 phosphorylated residues. Recombinant MBP-CDK8 was incubated with different His-AHL10 variants (His-AHL10^{S313A}, His-AHL10^{S314A}, His-AHL10^{S317A}, His-AHL10^{S314A/S317A} and His-AHL10^{S313A/S314A/S317A}). **c** Phos-tag mobility assay showing salt-induced phosphorylation of AHL10 is partially dependent on CDK8 in vivo. Total proteins were extracted from 10-day-old seedlings of *AHL10-GFP/WT* and *AHL10-GFP/cdk8* with and without NaCl treatment. AHL10-GFP protein was immunoprecipitated by GFP-Trap agarose. Immunoblots were performed with anti-GFP antibody. Two independent

experiments were conducted with similar results. Immunoblots showing the AHL10-GFP protein abundance in *AHL10-GFP/ah10* (**d**), *AHL10^{S314A}-GFP/ah10* (**e**), *AHL10^{S314D}-GFP/ah10* (**f**) and *AHL10-GFP/cdk8* (**g**) transgenic seedlings treated with or without NaCl. Actin was used as a control. AHL10-GFP was detected with an anti-GFP antibody. The intensity of each band was measured using Image J software. **h** Relative protein levels of AHL10-GFP in (**d-g**). Three independent experiments were provided for the data statistics. Values are means \pm SD ($n = 3$). Different letters indicate statistically significant differences by one-way ANOVA (Tukey's multiple comparisons test, * $P < 0.05$, ** $P < 0.01$).

Fig. 11b, c). The primary root length of the double mutant was notably shorter, paralleling the root length measured in the *cdk8-1* single mutant (Fig. 5a, b, Supplementary Fig. 11d). These growth impairments highlighted a survival disadvantage for the *cdk8-1* *ah10* double mutant and *cdk8* single mutant, with survival rates that were significantly lower

than those of both the WT and the *ah10* mutant in salt-treated soil (Fig. 5c, d).

To study if the phosphorylation of AHL10 affects salt tolerance, we generated complementary transgenic lines that carried various mutant forms of AHL10 under the control of its native promoter

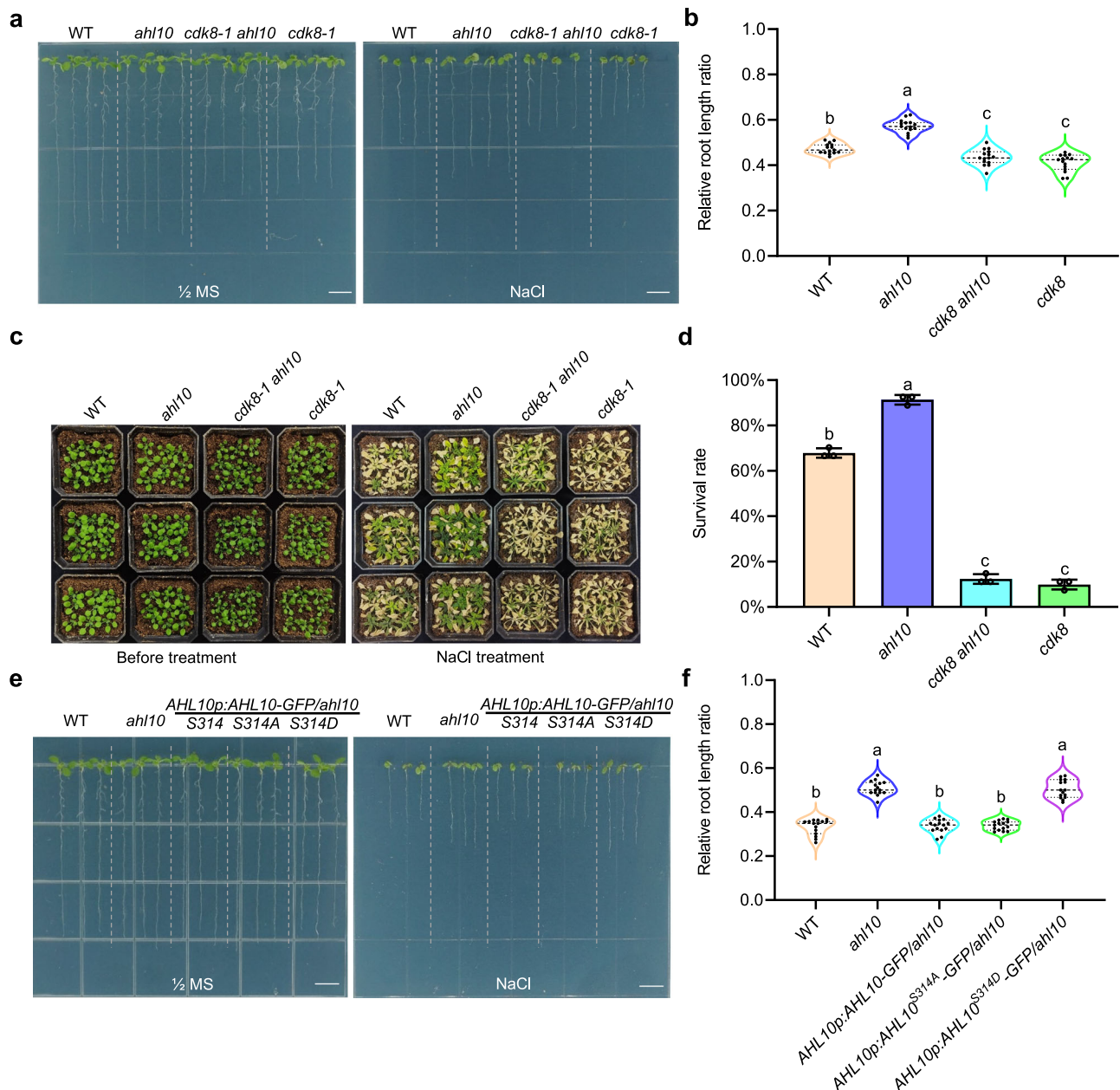


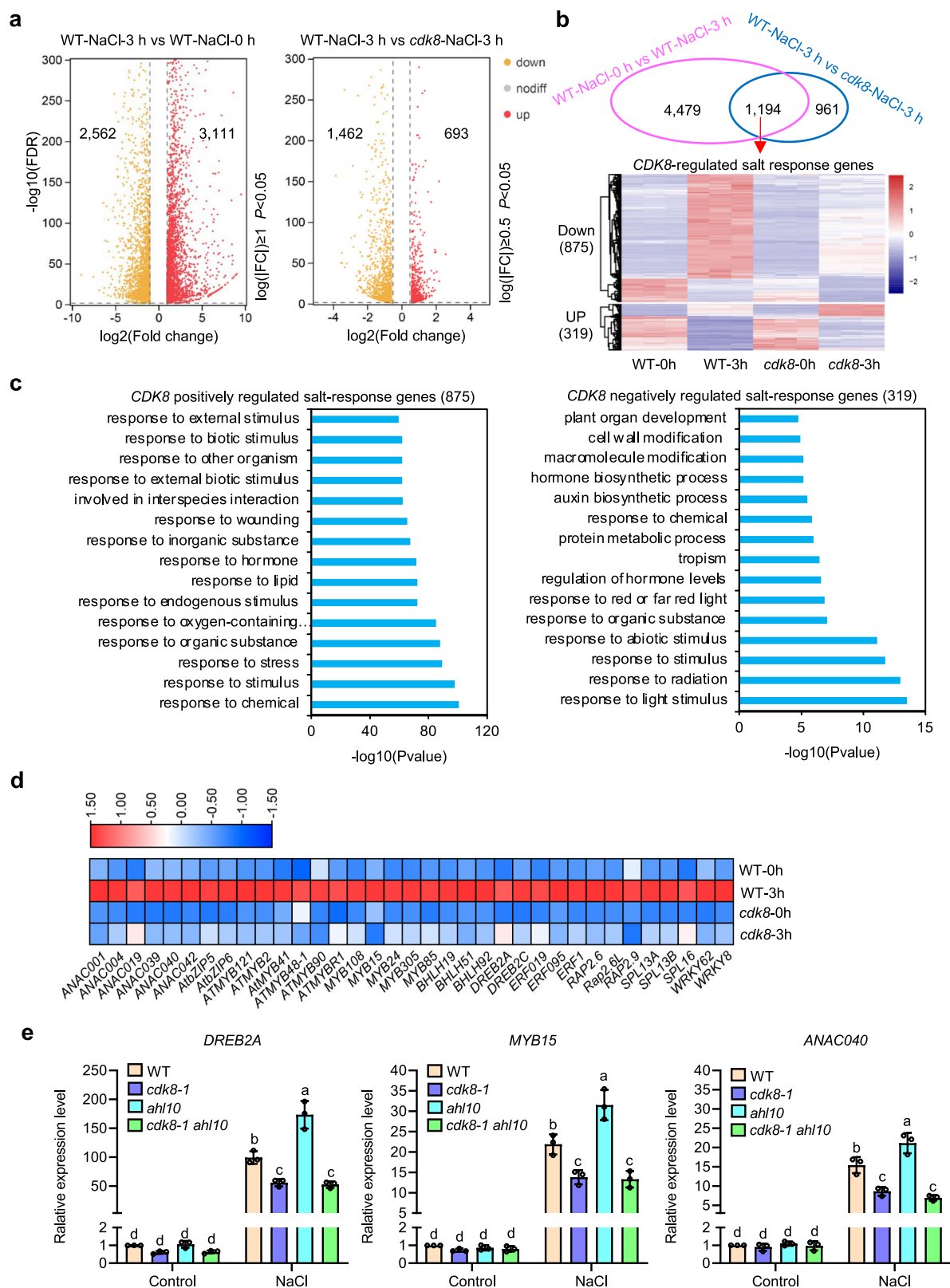
Fig. 5 | The phosphorylation of AHL10's Ser314 is required for CDK8 to promote salt stress response. **a** The root growth of the WT, *ah10*, *cdk8-1 ah10* and *cdk8-1* mutant seedlings on 1/2 MS plates with or without 0.1 M NaCl. **b** Relative primary root length ratio of the WT, *ah10*, *cdk8-1 ah10* and *cdk8-1* mutant seedlings in (h). Values are means \pm SD ($n = 15$). Different letters indicate statistically significant differences by one-way ANOVA (Tukey's multiple comparisons test, $P < 0.01$). **c** The salt tolerance phenotype of WT, *ah10*, *cdk8-1 ah10* and *cdk8-1* mutant seedlings grown in soil. **d** Survival rate corresponding to (c). Values are means \pm SD from three independent replicates. Different letters indicate statistically significant

differences by one-way ANOVA (Tukey's multiple comparisons test, $P < 0.01$). **e** The root growth phenotype of the WT, *ah10*, *AHL10p:AHL10^{S314A}-GFP/ah10*, *AHL10p:AHL10^{S314D}-GFP/ah10* and *AHL10p:AHL10^{S314A}-GFP/ah10* transgenic plants on 1/2 MS plates with or without 0.1 M NaCl. **f** Relative primary root length ratio of the WT, *ah10*, *AHL10p:AHL10^{S314A}-GFP/ah10*, *AHL10p:AHL10^{S314D}-GFP/ah10* and *AHL10p:AHL10^{S314A}-GFP/ah10* transgenic seedlings in (e). Values are means \pm SD ($n = 15$). Different letters indicate statistically significant differences by one-way ANOVA (Tukey's multiple comparisons test, $P < 0.01$).

(Supplementary Fig. 10). We demonstrated that the salt insensitivity of *ah10* mutants could be restored by *AHL10pro:AHL10/ah10* and *AHL10pro:AHL10^{S314A}/ah10*. The primary root lengths and green cotyledon percentages of *AHL10pro:AHL10/ah10* and *AHL10pro:AHL10^{S314A}/ah10* transgenic plants were comparable to the WT under salt treatment. In contrast, *AHL10pro:AHL10^{S314D}/ah10* transgenic plants failed to complement the salt phenotype of *ah10* mutants (Fig. 5e, f, Supplementary Fig. 12a, b, c), further indicating that Ser314 of AHL10 is critical for its function in regulating salt tolerance.

CDK8 regulates transcriptional reprogramming of salt stress-responsive genes

To understand the molecular mechanism by which *CDK8* regulates salt stress response, we used WT and *cdk8-1* mutant seedlings treated with distilled water and NaCl to perform RNA sequencing (RNA-seq). In the WT, 5,673 genes were identified as salt stress-responsive genes and 2,155 genes exhibited patterns of differential expression between the WT and *cdk8* mutants after salt stress. Of these, 1,194 genes overlapped and we classified them as *CDK8*-regulated salt-responsive



genes, accounting for more than 20% of the salt-responsive genes (Fig. 6a and Supplementary Data 2). According to the heatmap created with *CDK8*-regulated salt-responsive genes, approximately 73.3% of these genes (875) were positively regulated by *CDK8*, whereas 26.7% (319) were negatively regulated by *CDK8* (Fig. 6b). Gene Ontology (GO) enrichment analysis further established that these *CDK8*-regulated salt responsive genes are mainly enriched in

the response to chemical, response to stimulus and response to stress (Fig. 6c).

Recent studies have identified several key genes implicated in the salt stress response, which include *MYB108*, *MYB15*, *BHLH92*, *ANAC40*, and *ANAC42*^{48–51}. Notably, these genes along with *DREB2A* and several *ETHYLENE RESPONSIVE FACTOR* (*ERF*) TFs were found to be down-regulated in *cdk8* mutant after salt treatment (Fig. 6d). RT-qPCR was

Fig. 6 | Transcriptome analysis of CDK8-regulated salt-responsive genes.

a Volcano plots representing the fold-change of DEGs in the comparison groups of WT-NaCl-0h vs WT-NaCl-3h and WT-NaCl-3h vs *cdk8*-NaCl-3h. Red and yellow dots represent up-regulated and down-regulated genes, respectively ($P < 0.05$, absolute fold change ≥ 1). Gray dots represent genes without significant changes. Statistical tests for differentially expressed genes were performed based on negative binomial distribution by DESeq2 software. **b** Venn diagrams and Heatmap representing DEGs regulated by *CDK8*. **c** Gene Ontology (GO) analysis showing the top 15 enrichment categories of *CDK8*-regulated salt-responsive genes. Results of classification in

biological process categories with P values from statistical overrepresentation test are presented ($FDR < 0.05$). P values are in exponential notation ($E + n$). **d** Heat map analysis of salt-responsive transcription factors regulated by *CDK8*. **e** Relative expression levels of *DREB2A*, *MYB15* and *ANACO40* in WT, *cdk8-1*, *ahl10* and *cdk8-1 ahl10* mutant plants with or without NaCl treatment. *ACTIN2* was used as a control. The expression of the indicated genes in untreated WT was set at 1. Data represent means \pm SD of three technical repeats. Different letters indicate statistically significant differences by two-way ANOVA (Tukey's multiple comparisons test, $P < 0.01$).

performed to further validate these findings, showing that the salt-induced expression of *DREB2A*, *MYB15* and *ANACO40* was significantly suppressed in both the *cdk8-1* and *cdk8-1 ahl10* double mutants (Fig. 6e). This suppression indicated a positive regulatory role of CDK8 in modulating the transcription of several salt responsive genes. We also examined the expression patterns of ion-associated proteins related to salt stress, specifically *SOS1*, *HKT1* and *NHX1* in the WT, *cdk8* and *ahl10* mutants. Our results revealed that salt stress notably induced the expression of *SOS1* and *NHX1*, but not *HKT1* in these three genotypes (Supplementary Fig. 13).

To further determine the role of AHL10 in salt stress response, we detected the expression patterns of selected salt stress-responsive genes in plants expressing different variants of AHL10. Utilizing RT-qPCR, our analysis revealed that the expression of key salt stress-responsive genes, *DREB2A*, *MYB15* and *ANACO40*, was enhanced in *ahl10* and *AHL10pro:AHL10^{S314D}* transgenic plants. In contrast, the expression levels of these genes in *AHL10pro:AHL10^{S314}* and *AHL10pro:AHL10^{S314A}* transgenic plants were comparable to those observed in WT (Supplementary Fig. 14). These results further demonstrated that the salt-induced phosphorylation and subsequent degradation of AHL10 play a pivotal role in actively regulating the expression of salt stress-responsive genes.

Identification of AHL10 binding motifs and AHL10-CDK8 co-regulatory target genes

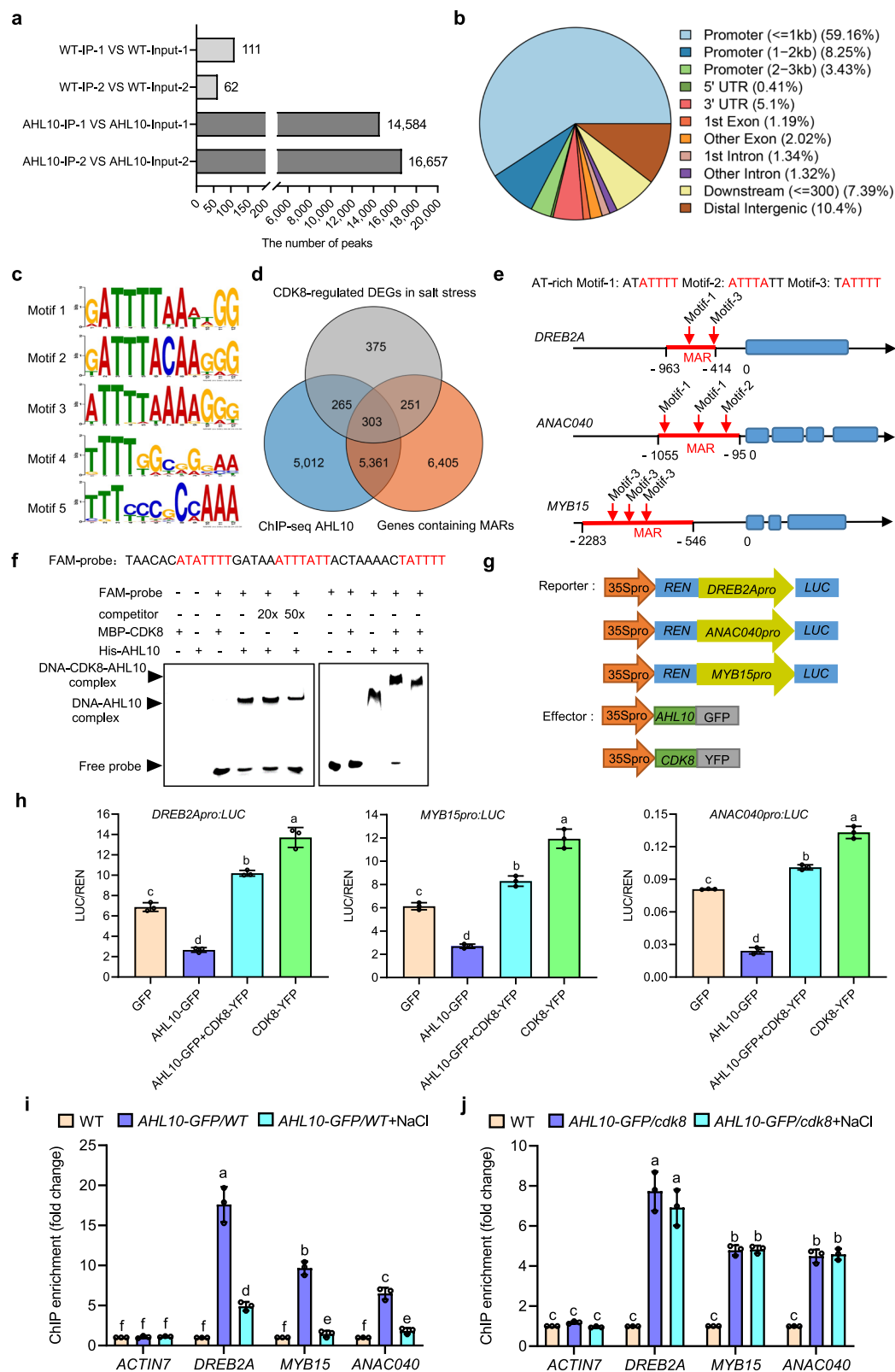
Our study also involved a thorough investigation into the binding patterns of the AHL10 protein. Chromatin immunoprecipitation sequencing (ChIP-seq) using AHL10-GFP transgenic plants was performed. To ensure the reliability and robustness of our findings, we conducted two independent biological replicates of this analysis. In the first replicate, we identified a total of 14,584 distinct genomic regions where the AHL10 protein was found to be strongly associated. The second replicate, carried out under identical experimental conditions, revealed 16,657 AHL10 binding peaks. The close agreement between these two independent data sets provided a high degree of confidence in the validity and reproducibility of our results (Fig. 7a). Notably, over 70% of these peaks were located in the promoter regions (Fig. 7b). These peaks were associated with a total of 12,803 genes, of which 10,941 genes were identified as having putative AHL10 binding sites (Supplementary Data 3). GO analysis additionally revealed the biological functions enriched among the putative target genes of AHL10. Biological processes of response to stimuli, response to chemicals, and response to stress were prominently featured. Moreover, major molecular functions associated with AHL10 binding included DNA-binding TF activity, transcriptional regulatory activity, transcriptional cis-element region binding, and RNA polymerase II regulatory region sequence-specific DNA binding were also featured (Supplementary Fig. 15). These findings suggested that AHL10-bound genes are likely integral to the transcriptional regulation of stress responses. Furthermore, we identified five top AHL10-binding motifs characterized by conserved contiguous T bases, such as motifs (G/A)ATTTT(A/T)A(A/T)(N)GG (Motif 1), (G/T)ATTACAA(N)(G/A)(G/A) (Motif 2), (A/T)TT(T/G)(T/A)(A/T)AAA(G/T)(N)₃ (Motif 3) (Fig. 7c). These results implied that the AHL10 protein preferentially bind with the motifs containing AT-rich regions.

Recent studies have highlighted the role of AHL proteins in binding to AT-rich DNA sequences⁵², particularly in association with nuclear matrix attachment regions (MARs)³³. Based on a previous report³², we focused on a comprehensive genome-wide analysis to identify genes containing MARs within the 2,000 bp upstream of their promoters. This analysis revealed a total of 12,320 genes (Supplementary Data 4). Given that we have demonstrated that CDK8 and AHL10 can differentially regulate salt tolerance, we aimed to develop deeper insights into the salt-responsive genes that these two proteins might coordinate. To achieve this, we used Venn Diagrams to comparatively analyze salt stress-responsive genes regulated by CDK8 alongside potential target genes of AHL10, and genes whose promoters contain MARs (Fig. 7d). We found that about 46% (554/1,194) of CDK8-regulated salt stress-responsive gene promoters contained MARs. Meanwhile, about 47% (568/1,194) of these CDK8-regulated salt-responsive genes were identified as AHL10-binding genes, showcasing a significant overlap between these regulatory pathways. Interestingly, our analysis revealed that about 51% (5,664/10,941) of the identified AHL10-binding genes also contain MARs, further highlighting the interconnectedness of these two genes. We further pinpointed 303 salt stress-responsive genes as potential co-regulated targets of AHL10 and CDK8 (Supplementary Data 5). This was supported by RT-qPCR validation, which demonstrated that the levels of key salt-responsive genes *DREB2A*, *ANACO40*, and *MYB15* were differentially expressed in *cdk8* and *ahl10* mutants (Fig. 6e).

CDK8 interferes with AHL10-mediated transcriptional repression of salt-responsive genes

The promoters of the salt-responsive genes *DREB2A*, *ANACO40*, and *MYB15* were found to contain MARs and potential AT-rich motifs that are putative binding sites for AHL10 (Fig. 7e). To explore the interaction between AHL10 and these elements, we utilized an electrophoretic mobility shift assay (EMSA). EMSA results confirmed that the recombinant His-AHL10, rather than MBP-CDK8 protein, was specifically bound to the FAM-labeled AT-rich oligonucleotide probe in vitro. This specificity suggests that AHL10 plays a crucial role in recognizing and interacting with the AT-rich motifs present in the promoter regions of these genes. At the same time, we found that when His-AHL10 was co-incubated with MBP-CDK8, a “super-shift” was detected (Fig. 7f), indicating that AHL10 and CDK8 may form a complex, potentially enhancing the regulatory effects on the salt-responsive genes. The formation of the AHL10-CDK8 complex may signify a coordinated mechanism by which these proteins modulate gene expression in response to salt stress.

To assess the transcriptional role of AHL10 in regulating those salt-responsive genes, we conducted dual luciferase reporter assays in Arabidopsis protoplasts and tobacco leaves. The assays employed three specific reporter constructs: *DREB2Apro:LUC*, *ANACO40pro:LUC* and *MYB15pro:LUC*. As effectors, we used *35Spro:AHL10-GFP* and *35Spro:CDK8-YFP* (Fig. 7g). Our results showed that the co-expression of AHL10-GFP effector significantly suppressed the LUC activities associated with all three reporter genes, indicating a strong inhibitory effect of AHL10 on salt-responsive gene activation. Conversely, the co-expression of the CDK8-YFP effector led to significant enhancement of LUC activity across all three reporter constructs (Fig. 7h,



Supplementary Fig. 16), suggesting that CDK8 plays a key role as a transcriptional activator. To further determine the effect of CDK8 on the transcription of AHL10-repressed genes, we explored the co-expression of AHL10-GFP and CDK8-YFP effectors. Our results demonstrated that this co-expression can partially relieve the inhibitory effects of AHL10 on the reporter genes (Fig. 7h, Supplementary Fig. 16).

To explore whether CDK8 and salt stress can affect the binding affinity of AHL10 to its target promoters, we performed ChIP-qPCR assays. Our findings unfolded a substantial enrichment of AHL10 at the promoters of *DREB2A*, *ANAC040* and *MYB15* in the *AHL10-GFP/WT* transgenic seedlings. However, this enrichment of AHL10 was markedly diminished after salt treatment (Fig. 7i). In contrast, we observed considerably lower enrichment of AHL10 at those same promoters in

Fig. 7 | AHL10-mediated transcriptional repression of *DREB2A*, *ANACO40* and *MYB15*. **a** ChIP-seq analysis identifies AHL10-enriched peaks. **b** Distribution of SIVOZ1 binding peaks across the *Arabidopsis* genome. **c** The five enriched binding motifs identified for AHL10. **d** Venn diagram identifies target genes co-regulated by AHL10-CDK8. **e** Schematic diagram of the MARs and potential AHL10 binding sites in *DREB2A*, *ANACO40* and *MYB15* promoters. Red lines indicate MARs; blue boxes indicate exons; red arrows indicate the location of AT-rich motifs on MARs. **f** EMSA showing the binding of AHL10 to the FAM-labeled AT-rich probe. **g** Schematic diagrams of the effector and reporter constructs used for the transactivation assay. **h** LUC/REN ratio showing CDK8 and AHL10-mediated transcriptional repression of

DREB2A, *ANACO40*, and *MYB15*. Values are means \pm SD ($n = 3$). Different letters indicate statistically significant differences by one-way ANOVA (Tukey's multiple comparisons test, $P < 0.01$). **i, j** ChIP-qPCR showing the enrichment of AHL10 at the MARs of *DREB2A*, *MYB15* and *ANACO40* promoters. WT, *AHL10-GFP/WT* and *AHL10-GFP/cdk8* seedlings were treated with and without NaCl. ChIP-qPCR data were normalized to internal inputs. *ACTIN7* was used as a control. Enrichment on the promoters of the indicated genes in WT was set to 1. Values are means \pm SD ($n = 3$). Different letters indicate statistically significant differences by two-way ANOVA (Tukey's multiple comparisons test, $P < 0.01$).

the *AHL10-GFP/cdk8* transgenic seedling. In the *cdk8* mutant background, no significant difference was found in the levels of AHL10 enrichment at those promoters either with or without the salt treatment (Fig. 7j). These results suggested that CDK8 interferes with AHL10 enrichment at the promoters of its targets.

AHL10 recruits SUVH2/9 to epigenetically regulate the transcription of salt stress-responsive genes via H3K9me2

Knowing that AHLs can be involved in chromatin modification, we next investigated whether AHL10 could regulate the transcription of salt-responsive genes through epigenetic mechanisms. Previous reports have indicated that AHL10 and SUVH9 may ectopically recruit H3K9me2 to AT-rich transposable elements (TEs), which subsequently leads to the repression of neighboring genes⁴¹. Considering that SUVH2 and SUVH9 are highly homologous and functionally redundant, we hypothesized that AHL10 may recruit SUVH2 and/or SUVH9 (SUVH2/9) to regulate transcriptional repression. To test our hypothesis, we first examined if AHL10 can interact with SUVH2/9. In our BiFC assays, we observed YFP fluorescence signals localized in the nucleus when nYFP-AHL10 was co-transformed with SUVH2/9-cYFP (Fig. 8a), indicating a potential interaction. Similarly, LCI assays revealed strong LUC activities following the co-infiltration of AHL10-cLUC with SUVH2/9-nLUC, further supporting this interaction (Supplementary Fig. 17). In addition, our Co-IP assays confirmed the presence of SUVH2/9-MYC fusion proteins following immunoprecipitation of AHL10-GFP when compared to negative controls. Interestingly, we found that salt stress led to a significant reduction in the protein levels of SUVH2/9 protein that were precipitated by AHL10-GFP (Fig. 8b). These findings thus indicated that AHL10 can form a complex with SUVH2/9.

To study the role of *SUVH2/9* in salt tolerance, we analyzed seed germination and post-germination seedling growth in the WT, *ahl10*, and *suvh2/9* mutants. Both the *ahl10* and *suvh2/9* mutants exhibited a significantly enhanced tolerance to salt stress compared to the WT, as evidenced by higher cotyledon greening (Supplementary Fig. 18a, b) and longer primary root length (Fig. 8c, d, Supplementary Fig. 18c). Moreover, the expression levels of salt-responsive genes *DREB2A*, *ANACO40*, and *MYB15* were up-regulated in the *suvh2/9* mutant (Supplementary Fig. 18 d). These findings revealed that SUVH2/9 functions as a negative regulator of salt tolerance.

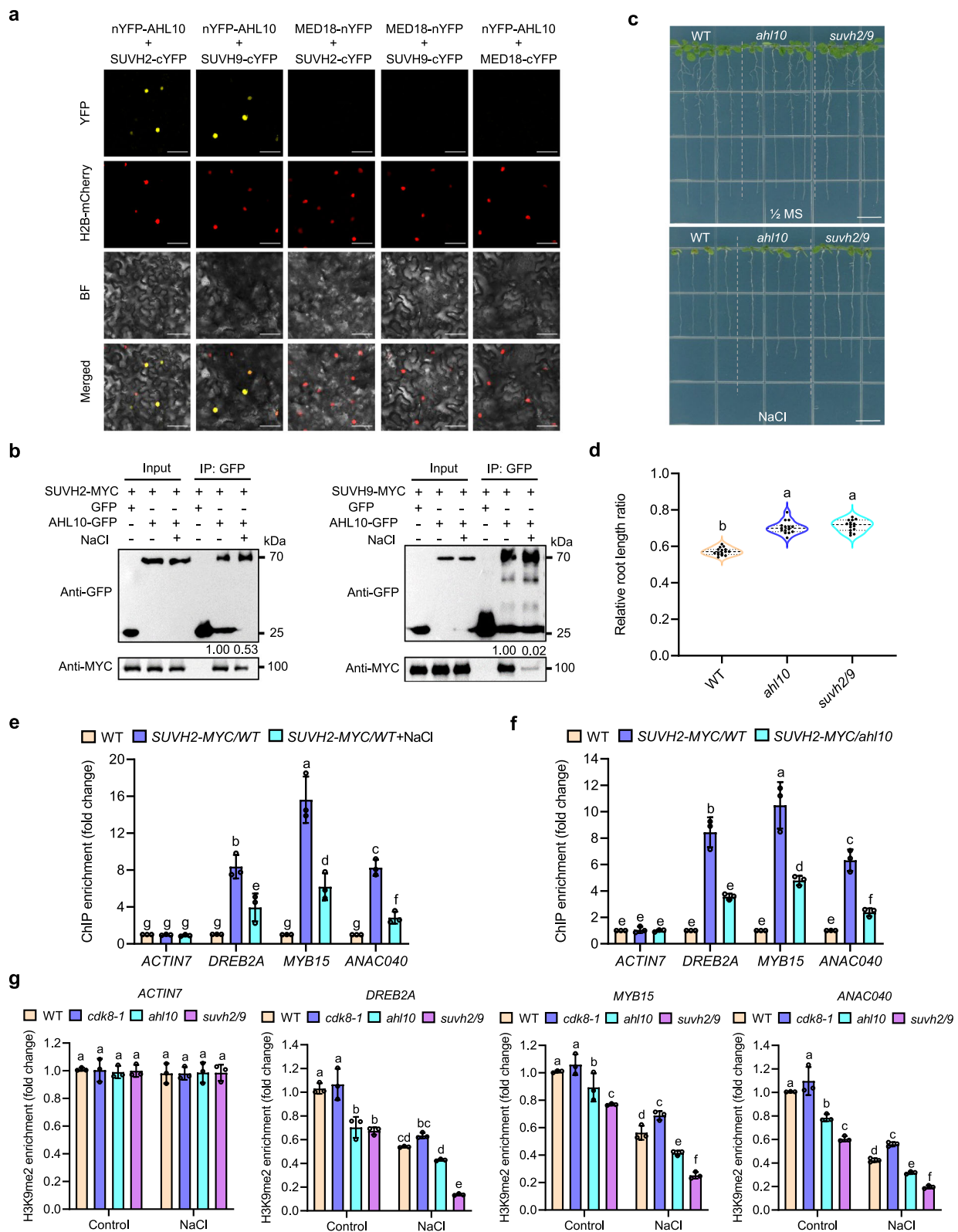
To investigate whether SUVH2/9 can be enriched at the promoters of salt stress-responsive genes, we conducted ChIP experiments using stable transgenic plants expressing *SUVH2/9-MYC*. We revealed that both SUVH2 and SUVH9 can be enriched at the MARs of the promoters of *DREB2A*, *MYB15*, and *ANACO40*. This enrichment, however, was diminished by salt stress treatment (Fig. 8e, Supplementary Fig. 19a). Given that AHL10 can interact with SUVH2/9, we then wanted to determine if AHL10 is required for the recruitment of SUVH2/9 to the target gene promoters. To address this, we performed additional ChIP experiments comparing *SUVH2/9-MYC/WT* with *SUVH2/9-MYC/ahl10* transgenic plants. The results showed that the enrichment of SUVH2/9 at the *DREB2A*, *MYB15*, and *ANACO40* promoters was repressed in the *ahl10* mutant background (Fig. 8f, Supplementary Fig. 19b). These observations implied that AHL10 is essential for facilitating the recruitment of SUVH2/9 to the promoters of salt responsive genes.

To understand how AHL10 coordinates with SUVH2/9 to regulate salt-stress responsive genes in an epigenetic manner, we examined the levels of H3K9me2 next as elevated H3K9me2 levels is an indicator of transcriptional repression⁴². In this context, it was essential to investigate the levels of H3K9me2 at the *DREB2A*, *MYB15*, and *ANACO40* promoters. ChIP-qPCR analysis revealed that *ahl10* and *suvh2/9* mutants exhibited significantly reduced levels of H3K9me2 at these promoters when compared to WT and *cdk8* mutants under both normal or salt stress conditions. In contrast, the *ACTIN7* promoter did not show significant variations in H3K9me2 levels across the different genotypes. Moreover, the salt-responsive target genes were observed to have lower H3K9me2 levels following salt treatment across all genotypes. Despite this pattern, the *cdk8* mutant showed relatively higher H3K9me2 levels compared to both WT and *ahl10* mutants (Fig. 8g). Collectively, these findings indicated that the CDK8-AHL10-SUVH2/9 module is associated with H3K9me2 modifications and thus plays an important role in the coordination of transcriptional responses to salt stress.

Discussion

Salt stress response involves a complex network of signaling pathways that trigger transcriptional reprogramming in plants. Aside from activating SOS signaling pathways to modulate salt stress responses, plants can also utilize diverse mechanisms to maintain the balance between transcriptional repression and activation of salt-responsive genes. Nevertheless, the key regulators that orchestrate these processes remain poorly understood. In our present work, we uncovered that the Mediator kinase subunit CDK8 and its substrate AHL10 function antagonistically in regulating salt tolerance and the transcriptional response triggered by salt stress. Specifically, we found that these regulators exert their effects through a mechanism mediated by SUVH2 and SUVH9, which are involved in the epigenetic modification of target genes. This epigenetic regulation allows for the fine-tuning of gene expression in response to salt stress, allowing plants to adapt to changing salinity levels.

Upon sensing a high presence of Na⁺ ions and a change in Ca²⁺, it is well known that plants can activate the Ca²⁺-CALCINEURIN B-LIKE PROTEIN (CBL)-CBL INTERACTING PROTEIN KINASE (CIPK) modules along with the SOS3-SOS2-SOS1 module to cope with salt stress^{1,53,54}. Our current findings have expanded our understanding of these adaptive responses by demonstrating that salt stress can also substantially stimulate the kinase activity of CDK8, a key regulator in the transcriptional machinery, and promote its phosphorylation of AHL10, leading to the degradation of AHL10. AHL10 is a conserved member of the AHL TF family in plants²⁷ and its phosphorylation status is essential for its biological function as it can be dephosphorylated by Highly ABA-Induced 1 (HAI1) to coordinate plant growth and osmotic stress responses³⁵. Despite the identification of multiple phosphorylation sites (Ser313, Ser314, and Ser317) on AHL10, the upstream protein kinases that modulate these phosphorylation events remain largely unexplored. Recent advances in phosphoproteomics have suggested that AHL10 may be a substrate of mitogen-activated protein kinases (MPKs), highlighting a potential regulatory pathway⁵⁵. However, the lack of thorough validation in these studies has left questions about

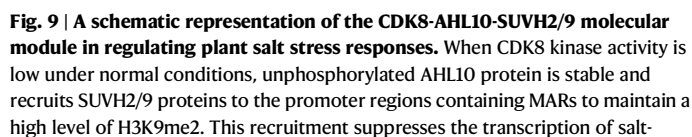


the specific mechanisms at play. Our work has provided biochemical and genetic evidence indicating that Ser314 is phosphorylated by CDK8 and this modification is critical for maintaining the protein's stability and functionality under salt stress.

We also demonstrated that AHL10 negatively regulates salt tolerance by repressing the expression of stress-responsive genes. Previous studies have highlighted the role of the *AHL* gene family in

binding to AT motif-rich DNA⁵², which is associated with MARs³³, and such interactions may facilitate chromatin modifications. In fact, certain members of the *AHL* gene family, *AHL22*, *SOB3/AHL29* and *MtAHL1*, have been shown to bind to AT motif-rich regions and regulate the expression of genes related to plant growth and development^{36–58}. From our transcriptomics data, we observed that almost half of the CDK8-regulated salt-responsive genes contain MARs. Moreover, our

revealing that the enrichment of SUVH2 in salt stress-responsive genes is dependent on AHL10. **g** ChIP-qPCR showing the fold enrichment of H3K9me2 at the MARs of *DREB2A*, *MYB15* and *ANAC040* promoters. WT, *cdk8-1*, *ahl10* and *suw2h/9* seedlings were treated with and without NaCl. ChIP-qPCR data were normalized to internal inputs. *ACTIN7* was used as a control. Enrichment on the promoters of the indicated genes in WT was set to 1. Values are means \pm SD ($n = 3$). Different letters indicate statistically significant differences by two-way ANOVA (Tukey's multiple comparisons test, $P < 0.01$).



responsive genes. Upon sensing salt stress, CDK8 becomes activated and triggers the phosphorylation of AHL10 to promote AHL10 protein degradation. As AHL10 levels decline, the recruitment of SUVH2/9 is also diminished, leading to a decrease in H3K9me2 levels in the promoter regions containing MARs and facilitating the transcriptional activation of salt-responsive genes.

Based on our findings, we proposed a working model for the regulation of salt tolerance by the CDK8-AHL10-SUVH2/9 module in plants. Under non-stress conditions, the kinase activity of CDK8 is relatively low. In this state, the AHL10-SUVH2/9 complex accumulates at the promoters of AT-rich DNA motifs, serving to repress the transcription of key salt-responsive genes. This repression is achieved

through the SUVH2/9 proteins, which enhance the deposition of repressive H3K9me2 histone modifications at these gene loci. Upon exposure to salt stress conditions, the kinase activity of CDK8 becomes activated and CDK8 proceeds to phosphorylate the AHL protein. This phosphorylation triggers the rapid degradation of AHL10, which subsequently disturbs the association between AHL10 and the SUVH2/9 complex. Without AHL10, SUVH2/9 can no longer maintain the repressive H3K9me2 marks at the salt-responsive gene promoters (Fig. 9). As a result, the transcriptional silencing is relieved, allowing the activation of these stress-responsive genes and the enhancement of the plant's salt tolerance. In conclusion, our study has uncovered the CDK8-AHL10-SUVH2/9 module as an important molecular switch that dynamically regulates the transcription of salt-responsive genes and salt tolerance in plants.

Plant materials and growth conditions

The transgenic *Arabidopsis* plants were generated by *Agrobacterium tumefaciens* (GV3101)-mediated floral dip transformation, including CDK8-YFP (35S:CDK8-YFP)²⁵, CDK8pro:GUS (CDK8pro:GUS)²⁶, AHL10-GFP (Super:AHL10-GFP), AHL10-GFP/ahL10 (Super:AHL10-GFP), AHL10^{S314A}-GFP/ahL10 (Super:AHL10^{S314A}-GFP), AHL10^{S314D}-

GFP/ahl10 (*Super:AHL10^{S314D}-GFP*), *AHL10-GFP/cdk8* (*Super:AHL10-GFP*), *AHL10pro:AHL10^{S314}/ahl10* (*AHL10pro:AHL10^{S314}-GFP*), *AHL10pro:AHL10^{S314A}/ahl10* (*AHL10pro:AHL10^{S314A}-GFP*), and *AHL10pro:AHL10^{S314D}/ahl10* (*AHL10pro:AHL10^{S314D}-GFP*). Transgenic plants were screened with hygromycin B, and validated by immunoblotting with anti-GFP antibody (Roch, 11814460001). To generate *AHL10* CRISPR-Cas9 lines (*ahl10-cr1*), we constructed the CRISPR-Cas9 vector as previously described⁵⁹. The gene editing site of *AHL10* was obtained through the online site (<http://crispor.tefor.net/>). T3 or T4 homozygous plants with desired mutations were utilized for this study.

The seeds were surface sterilized with 10% NaClO for 20 min, followed by at least three washes with distilled water. After 3 days at 4 °C, the seeds were germinated on 1/2 Murashige and Skoog (1/2 MS) medium supplemented with 1.5% (w/v) sucrose at 22 °C, 60–80% relative humidity with a light/dark cycle of 16 h/8 h. 4-week-old *Nicotiana benthamiana* (*N. benthamiana*) plants were grown in soil under a 12-h light/12-h dark cycle at 25 °C were utilized for transient transformation.

Salt stress treatment

In the seed germination assay, at least 100 seeds were germinated on 1/2 MS medium with or without 0.1 M NaCl, and the greening percentage of cotyledons was calculated after 5 days. In the primary root elongation experiment, seeds were first germinated on 1/2 MS medium for 3 days and then transferred to 1/2 MS medium with or without 0.1 M NaCl for 5 days before measuring the primary root length. Salt stress survival experiments were conducted as follows: plants were grown in soil for 2 weeks under a 16-h light/8-h dark cycle, during which time the soil moisture content was controlled at 60%. Plants were then subjected to salt stress for 2 or 3 weeks, during which time they were treated 2 or 3 times with 0.2 M NaCl solution and the soil water content was controlled at 60%. After the salt treatment, plants were allowed to recover for 2 weeks, during which time the soil water content was controlled at 60% using deionized water, and then survival was recorded.

GUS staining

The GUS staining buffer was prepared according to the instructions of the GUS staining kit (Coolaber, SL7160). 7-day-old *CDK8pro:GUS* seedlings were treated with water or 0.2 M NaCl for 3 h before immersed in GUS staining buffer and incubated at 37 °C in the dark for 3 h. Chlorophyll was subsequently removed with 70% ethanol. The stained seedlings were observed and photographed using a stereomicroscope (Olympus, szx7).

Plasmid construction

The full-length or truncated coding sequences of *CDK8* and *AHL10* were amplified with PrimeSTAR MAX (Takara) and were cloned into several vectors including *pSuper1300* (MYC and GFP-tag), *pET28a* (His), *PXY106-nYFP*, *PXY104-cYFP*, *pCAMBIA1300* (nLUC or cLUC), *pGBKT7* (BD), and *pGADT7* (AD). To obtain point mutation constructs such as *His-AHL10^{S313A}*, *His-AHL10^{S314A}*, *His-AHL10^{S314D}*, *His-AHL10^{S317A}*, *His-AHL10^{S314A/S317A}*, and *His-AHL10^{S313A/S314A/S317A}*, we employed *His-AHL10* as the template. We designed amino acid mutation primers and performed PCR amplification of the mutant plasmids. Subsequently, we utilized DpnI to digest the template plasmids and then transformed them into *E. coli* for sequencing and identification. The native promoter sequence (about 2,680 bp) upstream of the *AHL10* was cloned into the *pCAMBIA1300-GFP* vector to generate *AHL10pro:GFP*. Subsequently, *AHL10^{S314}*, *AHL10^{S314A}*, and *AHL10^{S314D}* sequences were cloned into *AHL10pro:GFP* to generate *AHL10pro:AHL10^{S314}-GFP*, *AHL10pro:AHL10^{S314A}-GFP*, and *AHL10pro:AHL10^{S314D}-GFP*. In order to make the *DREB2A::LUC*, *MYB15::LUC*, *ANAC040::LUC* reporter vectors, the 1,000 bp promoter sequence of *DREB2A*, *MYB15* and *ANAC040* was amplified and cloned into the pGreenII 0800 vector. All constructed plasmids were verified by sequencing (Sangon Biotech). All primers used for plasmid construction are listed in Supplementary Data 6.

Sequence analysis

The DNA sequences of *AHL10* gene were obtained from TAIR (<https://www.arabidopsis.org/>). Sequence alignment and primer design using MEGA 7 and Primer Premier 5, respectively⁶⁰. Identification and mapping of MAR regions within the Arabidopsis thaliana genome were performed according to the procedures described³². A Linux program script was employed to extract DNA sequences with established physical positions and map them onto the 2,000 bp upstream region of the *Arabidopsis* genome-wide promoter.

Phosphoproteomics analysis

For Phosphoproteomics analysis, total protein was extracted from ten-day-old wild-type (WT) seedlings using a lysis buffer containing 6 M guanidine hydrochloride (GdnHCl), 100 mM Tris-HCl (pH 8.5), 10 mM tris(2-carboxyethyl)phosphine hydrochloride (TCEP), 40 mM 2-chloroacetamide (CAA), and a phosphatase inhibitor cocktail (ref.). Approximately 200 µg of protein extract was purified and alkylated by methanol-chloroform precipitation and dissolved in 12 mM sodium deoxycholate (SDC) and 12 mM sodium lauroyl sarcosinate (SLS). Protein digestion was performed using trypsin (Promega) at a 1:100 (w/w) enzyme-to-protein ratio, incubating at 37 °C overnight. The resulting peptides were desalted using SDB-XC StageTips^{45,61}.

For kinase reaction, desalted peptides were incubated with recombinant CDK8 kinase in a reaction buffer containing 50 mM Tris-HCl (pH 7.5), 10 mM MgCl₂, 1 mM dithiothreitol (DTT), and 1 mM γ-[¹⁸O₄]ATP at 30 °C overnight. Parallel reactions were conducted using MBP-CDK8 as the kinase and AHL10 as the substrate under identical buffer conditions. Kinase reactions were quenched by adding 1% trifluoroacetic acid (TFA). The ¹⁸O-labeled phosphopeptides were further digested with Lys-C at 37 °C for 6 h and subsequently enriched using Fe-IMAC.

For Fe-IMAC enrichment, custom IMAC tip were prepared by inserting a 20-µm polypropylene frit disk into the tip and filling it with 10 mg of nickel-nitrilotriacetic acid silica resin (Qiagen). Initially, Ni²⁺ ions were stripped by introducing 100 mM EDTA (200 g, 1 min). The tip was then primed with 100 mM FeCl₃ and balanced with 0.5% (v/v) acetic acid at pH 3.0 prior to sample application. Tryptic peptides, dissolved in 0.5% (v/v) acetic acid, were introduced into the IMAC tip. The tip was rinsed with 1% (v/v) TFA, 80% (v/v) ACN (200 g, 1 min), and 0.5% (v/v) acetic acid (pH 3.0). Following this, the Fe-IMAC tip was connected to an activated desalting SDB-XC (3 M) StageTip. Phosphopeptides bound to the tip were released onto the desalting Tip using 200 mM NH₄H₂PO₄ and directly collected into sample vials for LC-MS/MS analysis. Eluted peptides were dried under vacuum prior to analysis.

LC-MS/MS analysis

Approximately 200 ng phosphopeptides were introduced into a nanoElute 2 liquid chromatography system (Bruker). Peptides were separated on a 25 cm pepsep column (25 cm × 75 µm ID) containing C18 resin (1.7 µm, 120 Å, Bruker). The mobile phase buffer consists of 0.1% formic acid (buffer A) in water with an eluting buffer of 0.1% formic acid in ACN (buffer B). A 45 min gradient was programmed to run at 2–22% buffer B for 31 min, 22–37% for 4 min, 37–80% for 5 min, and 80% for 5 min. The LC system was coupled to a hybrid TIMS quadrupole TOF mass spectrometer (Bruker timsTOF Pro2) via a CaptiveSpray nano-electrospray ion source. Data acquisition was performed in data-dependent acquisition (DDA) mode with parallel accumulation-serial fragmentation (PASEF). The dual TIMS configuration utilized a ramp time and accumulation time of 100 ms, resulting in a total cycle time of 1.17 s. DDA-PASEF mode with 10 PASEF scans covered a mass range from 100 m/z to 1,700 m/z with charge states set from 0 to 5. The capillary voltage was set at 4,500 V. The ion mobility range was 0.7–1.3 Vs/cm². Dynamic exclusion was set to 0.4 min. The quadrupole isolation width was set to 2 Th for m/z < 700 and 3 Th for m/z > 800.

Analysis of the raw data was performed using MaxQuant version 2.2.0.0, which extracts four-dimensional features on the MS1 level

(retention time, m/z, ion mobility and intensity) and links them to peptide spectrum matches. Spectra were searched using the TAIR10 database with trypsin set as the enzyme (cleavage next to arginine or lysine, but not before proline) and the maximum number of missed cleavages set to 2. Carbamidomethyl (C) was set as a fixed peptide modification. Static modifications were oxidation (M), acetyl (protein N termini), Ser/Thr/Tyr phosphorylation (+79.996 Da) and 18O-phos(+85.979 Da). The maximum precursor mass tolerance of the main search was set to 20 ppm and deisotoping of fragment ions was deactivated. Peptides were accepted with a minimum length of 7 amino acids and a maximum size of 4.6 kDa. The processed data were filtered by posterior error probability to achieve a protein false discovery rate (FDR) of 1% and a peptide spectrum match FDR of 1%⁴⁵.

Phosphorylation site identification

To identify the specific amino acids of AHL10 phosphorylated by CDK8, recombinant protein MBP-CDK8 was mixed with His-AHL10 in a total volume of 30 μ L reaction buffer containing 25 mM Tris-HCl (pH 7.5), 12 mM MgCl₂, 1 mM DTT, and 1 mM ATP. The reaction mixture was incubated at 30 °C for 1 h before adding SDS-loading buffer. After SDS-PAGE, His-AHL10 protein glue strips were extracted for mass spectrometry analysis.

Y2H assay

The coding sequence of genes was amplified and introduced into GAL4-BD and GAL4-AD plasmids for transformation in Y2H Gold cells grown on the SD/-Trp-Leu deficient medium. The transformed yeast clones were subsequently plated on the SD/-Trp-Leu-His deficient media to determine the protein-protein interactions⁶².

BiFC assay

The coding sequence of *CDK8*, *AHL10*, *SUVH2* and *SUVH9* was amplified and cloned into pXY-106 vector (nYFP) or pXY-104 (cYFP)⁶³. The plasmids were introduced into *Agrobacterium* (GV3101) competent cells and the indicated plasmids were co-infiltrated in *N. benthamiana* leaves for transient transformation. After 48 h, the YFP and the nuclear marker H2B-mCherry signals were visualized by confocal microscopy (Zeiss LSM-980).

LCI assay

The constructed nLUC and cLUC plasmids were transformed into *Agrobacterium* (GV3101), and *Agrobacterium* strains were infiltrated into fully expanded leaves of *N. benthamiana*⁶⁴. After infiltration for 3 days, the leaves were sprayed with firefly luciferase substrate buffer (0.3 mg/mL D-Luciferin, Sodium Salt (YESEN, 40901ES01) and 0.1% Triton X-100), and the LUC activities were captured by Tanon 5200 Multi imaging system (Tanon Science and Technology, China). Total proteins were extracted for immunoblot analysis. nLUC and cLUC fusion proteins were detected with anti-luciferase antibody (Sigma, L0159, diluted 1:5000) and anti-cLUC antibody (Biodragon, BD-PM3656, diluted 1:5000), respectively.

Co-IP assay

Agrobacterium (GV3101) was transformed with the relevant plasmids before using them to infiltrate tobacco leaves. After 48 h of expression, total proteins were extracted with extraction buffer (50 mM Tris-HCl (pH 7.5), 150 mM NaCl, 1 mM EDTA (pH 8.0), 1 mM DTT, 1 mM PMSF, EDTA-free protease inhibitor cocktail (Roche, 11873580001) and 0.2% Triton X-100). The protein extract was next incubated with MYC-Trap or GFP-Trap agarose (Chromotek) for at least 3 h at 4 °C. After washing with IP buffer 5 times, the protein samples were mixed with SDS-loading buffer for 10 min at 95 °C. The proteins were detected by immunoblot using anti-MYC (Abcam, ab9106, diluted 1:5000) and anti-GFP antibodies (Roche, 11814460001, diluted 1:4000).

RNA extraction and RNA-seq analysis

Ten-day-old wild type (WT) and *cdk8-1* mutant seedlings grown on 1/2 MS plates were treated with or without 0.3 M NaCl for 3 h at room temperature. Total RNA was isolated using the RNAiso Reagent (Takara, T9108). NanoDrop 2000 spectrophotometer and Agilent 2100/ LabChip GX were used to detect the purity and concentration of RNA and the integrity of RNA, respectively. RNA-seq was performed by Biomarker Technologies (Beijing, China). DESeq2 software was used for differentially expressed gene (DEG) analysis with Fold Change ≥ 1.5 and False Discovery Rate (FDR) < 0.05 . Gene ontology (GO) enrichment analysis was performed using an online tool (<https://www.geneontology.org/>). The RNA-seq data was deposited at NCBI (PRJNA950536). Heatmap were generated by the TBtools software, employing the FPKM values of the genes and then normalizing them⁶⁵.

Quantitative reverse transcription PCR (RT-qPCR)

Total RNA was extracted from 10-day-old seedlings using RNAiso Reagent, followed by first-strand cDNA synthesis using PrimeScript RT Reagent Kit (Takara, RR047A). Quantitative PCR was performed using Hieff qPCR SYBR Green Master Mix Kit (YEASEN, 11201ES08) in QuantStudio 5 instrument (Applied Biosystems, USA)⁶⁶. Primer sequences are provided in Supplementary Data 6.

Phos-tag™ mobility shift assay

The experiments were carried out as described in the Phos-tag™ SDS-PAGE GUIDEBOOK (Wako, cat# AAL-107). To detect the phosphorylation of AHL10 proteins in vitro, 1 μ g of MBP-CDK8 was mixed with 1 μ g of His-AHL10 or its mutant form in a total volume of 30 μ L of reaction buffer containing 25 mM Tris-HCl (pH 7.5), 12 mM MgCl₂, 1 mM DTT, and 1 mM ATP. The reaction mixture was incubated at 30 °C for 1 h before boiling for 10 min. The samples were then separated by SDS-PAGE with and without 100 μ M Phos-tag™ and 100 μ M MnCl₂, followed by immunoblotting analysis using anti-His (Abcam, ab18184, diluted 1:5000) and anti-MBP (Proteintech, 15089-1-AP, diluted 1:5000) antibodies, respectively.

In vivo phosphorylation assay

Total protein was extracted from about 0.2 g of *AHL10-GFP/WT* and *AHL10-GFP/cdk8* seedlings with or without 0.2 M NaCl treatment using protein extraction buffer: 50 mM Tris-HCl (pH 7.5), 150 mM NaCl, 1 mM EDTA (pH 8.0), 1 mM DTT, 0.2% Triton X-100, EDTA-free protease inhibitor cocktail (Roche 11873580001), phosphatase inhibitor mixture (Sigma-Aldrich, PPC1010), 1 mM PMSF. Total protein was incubated with GFP-Trap agarose at 4 °C for at least 6 h. The agarose was then washed at least three times with the extraction buffer before denatured by adding SDS-loading buffer for 10 min at 95 °C. The proteins were separated on gels with and without 100 μ M Phos-tag™ and 100 μ M MnCl₂. The mobility shift was determined by immunoblotting analysis with anti-GFP antibody (Roche, 11814460001, diluted 1:4000).

In vivo protein stability assay

Seven-day-old seedlings of *AHL10-GFP/ahl10*, *AHL10-GFP/cdk8*, *AHL10^{S314A}-GFP/ahl10*, and *AHL10^{S314D}-GFP/ahl10* transgenic seedlings were treated with 100 μ M CHX or 100 μ M CHX plus 0.2 M NaCl for 0, 1, 3, 6, 9, and 12 h. The proteasome inhibitor MG132 was used as a control. Total protein was extracted using protein extraction buffer (50 mM Tris-HCl (pH 7.5), 150 mM NaCl, 1 mM EDTA (pH 8), 1 mM DTT, 0.2% Triton X-100, EDTA-free protease inhibitor cocktail (Roche 11873580001), 1 mM PMSF) and then denatured by adding SDS-loading buffer for 10 min at 95 °C. The samples were subjected to SDS-PAGE and western blotting using anti-GFP (Roche, 11814460001, diluted 1:4000) and anti-Actin (Sigma, A0840, diluted 1:10000) antibodies, with Actin serving as a loading control.

Analysis of the CDK8 kinase activity

Ten-day-old *CDK8-YFP* seedlings were treated with H₂O or 0.2 M NaCl for 1, 3 and 6 h. Total protein was extracted with protein extraction buffer. After centrifugation, the supernatant was incubated with GFP-Trap agarose at 4 °C for 4 h followed by washing twice with wash buffer (50 mM Tris-HCl (pH 7.5), 150 mM NaCl and 0.5 mM EDTA) and twice with PBS buffer. The immunoprecipitated proteins were incubated in 25 µl kinase buffer containing 50 mM HEPES (pH 7.5), 5 mM MgCl₂, 1 mM DTT and 1 mM ATP-γ-S (Abcam, ab138911) for 30 min at room temperature. The 2.5 mM p-Nitrobenzyl mesylate (Abcam, ab138910) was added and incubated at room temperature for 2 h⁶⁷. After the reaction, SDS-loading buffer was added for 10 min at 95 °C to terminate the reaction. Autophosphorylation of CDK8 was detected by western blotting using anti-thiophosphate ester antibody (Abcam, ab92570, diluted 1:5000).

Electrophoretic mobility shift assay (EMSA)

The FAM (5-carboxyfluorescein)-labeled oligonucleotide was synthesized as a probe⁶⁸. Briefly, the recombinant His-AHL10 protein was incubated with the probe in EMSA binding buffer containing 20 mM Tris-HCl (pH 7.5), 0.1 M NaCl, 2 mM MgCl₂, 1 mM DTT, 10% glycerol for 30 min at 4 °C. Subsequently, the samples were separated by 8% non-denaturing polyacrylamide gel. Fluorescence images were recorded with Tanon 5200 Multi imaging system.

Dual-luciferase reporter assay

LUC Reporters (*DREB2Apro::LUC*, *ANAC040pro::LUC* and *MYB15pro::LUC*) were co-expressed with or without effector *AHL10-GFP* in tobacco cells for 3 days. Firefly luciferase substrate (D-Luciferin, Potassium Salt (YESEN, 40902ES09) was sprayed, and the LUC activity signal Images were visualized by Tanon-5200 Multi Imaging System (Tanon Science and Technology, China). For the dual-luciferase gene reporter assay, reporter factors (*DREB2Apro::LUC*, *ANAC040pro::LUC* and *MYB15pro::LUC*) were co-expressed with or without effectors *AHL10-GFP* in tobacco cells for 3 days. The LUC and REN signals were detected by Hybrid Multi-Mode Microplate Reader (Tecan Trading AG, Switzerland).

ChIP-qPCR analysis

About 2 g seedlings was collected from 10-day-old WT, *AHL10-GFP/WT*, *AHL10-GFP/cdk8*, *SUVH2-MYC/WT*, *SUVH2-MYC/ahl10*, *SUVH9-MYC/WT*, and *SUVH9-MYC/ahl10*, seedlings for crosslinking with 1% formaldehyde. For NaCl treatment, 10-day-old WT, *AHL10-GFP/WT*, *AHL10-GFP/cdk8*, *SUVH2-MYC/WT*, and *SUVH9-MYC/WT* seedlings were treated with 0.2 M NaCl for 3 h before cross-linking. Chromatin complexes were incubated with GFP-Trap or MYC-Trap agarose at 4 °C for at least 6 h. Purification of DNA was carried out by adding 10% Chelex-100 and boiling for 10 min⁶⁹. ChIP-qPCR was repeated at least three independent replicates.

For ChIP-qPCR analysis of H3K9me2 in WT, *cdk8-1*, *ahl10* and *suvh2/9*. WT, *cdk8-1*, *ahl10* and *suvh2/9* seedlings treated with and without 0.2 M NaCl for 3 h were fixed, and then the samples' chromatin was extracted, sonicated, and immunoprecipitated by anti-H3K9me2 (Abcam, ab1220). Purified and recovered DNA was used for RT-qPCR, and each value was normalized to the control WT without NaCl treatment. ChIP-qPCR primer sequences are provided in Supplementary Data 6.

ChIP sequencing

About 2 g seedlings was collected from 10-day-old WT and *AHL10-GFP/WT* seedlings for crosslinking with 1% formaldehyde for 15 min, then treated with 2 M glycine for 5 min. Nuclear proteins were extracted, and genomic DNA was fragmented to approximately 250 bp by sonication (Diagenode). Samples were then diluted and immunoprecipitated overnight with GFP-Trap agarose beads (Chromotek). After washing the beads with buffers of low-salt wash buffer, high-salt wash

buffer, LiCl wash buffer, and TE buffer for 5 min each at 4 °C, DNA was extracted by a DNA extraction kit. DNA libraries were prepared using the NEBNext® Ultra™ II DNA Library Prep Kit for Illumina® (NEB, #E7645), and 150 bp paired-end deep sequencing was performed on the Illumina HiSeq/Novaseq⁷⁰. ChIP-seq was performed in two independent replicates. For all ChIP-seq data sets, raw data in fastq format are processed by Cutadapt (version 1.9.1) into high-quality clean data. Cleaned reads were aligned to the Arabidopsis genome (TAIR 10) via Bowtie2 v2 (version 2.2.6). Use MACS (V2) to analyze peaks quality control, peaks calling and peaks annotation. To identify conserved motifs in the AHL10 binding region, 500 bp of sequence around each consensus peak was extracted and submitted to the MEME-ChIP online version. GOSec (v1.34.1) is used identifying Gene Ontology (GO) terms that annotate a list of enriched genes with a significant qvalue (fdr, padj) less than 0.05.

Statistical analyses

Statistical significances between various groups were conducted according to the two-tailed Student's *t* test or one-way ANOVA or two-way ANOVA followed by Tukey's multiple range tests. All analyses were performed by GraphPad Prism 8.4.3.

Reporting summary

Further information on research design is available in the Nature Portfolio Reporting Summary linked to this article.

Data availability

Identifiers for published or publicly available lines are provided in Methods. Sequence data from this article can be found in GenBank/EMBL databases under the following accession numbers: CDK8 (AT5G63610), AHL10 (AT2G33620), SUVH2 (AT2G33290), SUVH9 (AT4G13460), ACTIN2 (AT3G18780), DREB2A (AT5G05410), MYB15 (AT3G23250), ANAC040 (AT2G27300) and ACTIN7 (AT5G09810). RNA-seq data have been deposited in the NCBI SRA database under BioProject [PRJNA950536](https://www.ncbi.nlm.nih.gov/bioproject/PRJNA950536). ChIP-seq data have been deposited in the NCBI SRA database under BioProject [PRJNA1105874](https://www.ncbi.nlm.nih.gov/bioproject/PRJNA1105874). The mass spectrometry proteomics raw data have been deposited with the ProteomeXchange Consortium via the PRIDE partner repository with the dataset identifier [PSX057837](https://www.ebi.ac.uk/pride/archive/study/PSX057837). All other relevant data are available from the corresponding author upon request. Source data are provided with this paper.

References

- Yang, Y. & Guo, Y. Elucidating the molecular mechanisms mediating plant salt-stress responses. *N. phytologist* **217**, 523–539 (2018).
- Yu, Z. et al. How Plant Hormones Mediate Salt Stress Responses. *Trends Plant Sci.* **25**, 1117–1130 (2020).
- Zhu, J. K. Abiotic Stress Signaling and Responses in Plants. *Cell* **167**, 313–324 (2016).
- Zhang, S. et al. Osmotic stress alters circadian cytosolic Ca(2+) oscillations and OSCA1 is required in circadian gated stress adaptation. *Plant Signal Behav.* **15**, 1836883 (2020).
- Yuan, F. et al. OSCA1 mediates osmotic-stress-evoked Ca²⁺ increases vital for osmosensing in Arabidopsis. *Nature* **514**, 367–371 (2014).
- Guo, Y., Halfter, U., Ishitani, M. & Zhu, J. K. Molecular characterization of functional domains in the protein kinase SOS2 that is required for plant salt tolerance. *Plant Cell* **13**, 1383–1399 (2001).
- Shi, H., Ishitani, M., Kim, C. & Zhu, J. K. The Arabidopsis thaliana salt tolerance gene SOS1 encodes a putative Na⁺/H⁺ antiporter. *Proc. Natl Acad. Sci. USA* **97**, 6896–6901 (2000).
- Zhu, J. K. Cell signaling under salt, water and cold stresses. *Curr. Opin. Plant Biol.* **4**, 401–406 (2001).
- Shi, H., Lee, B. H., Wu, S. J. & Zhu, J. K. Overexpression of a plasma membrane Na⁺/H⁺ antiporter gene improves salt tolerance in Arabidopsis thaliana. *Nat. Biotechnol.* **21**, 81–85 (2003).

10. Moller, I. S. et al. Shoot Na⁺ exclusion and increased salinity tolerance engineered by cell type-specific alteration of Na⁺ transport in Arabidopsis. *Plant Cell* **21**, 2163–2178 (2009).
11. Zhang, J. L. & Shi, H. Physiological and molecular mechanisms of plant salt tolerance. *Photosynth Res* **115**, 1–22 (2013).
12. Zhao, C. et al. Leucine-rich repeat extensin proteins regulate plant salt tolerance in Arabidopsis. *Proc. Natl Acad. Sci. USA* **115**, 13123–13128 (2018).
13. Zhao, C. et al. The LRXs-RALFs-FER module controls plant growth and salt stress responses by modulating multiple plant hormones. *Natl Sci. Rev.* **8**, nwaal49 (2021).
14. Liu, X. et al. FERONIA coordinates plant growth and salt tolerance via the phosphorylation of phyB. *Nat. Plants* **9**, 645–660 (2023).
15. Nakashima, K. et al. Organization and expression of two Arabidopsis DREB2 genes encoding DRE-binding proteins involved in dehydration- and high-salinity-responsive gene expression. *Plant Mol. Biol.* **42**, 657–665 (2000).
16. Kim, S. G., Kim, S. Y. & Park, C. M. A membrane-associated NAC transcription factor regulates salt-responsive flowering via FLOWERING LOCUS T in Arabidopsis. *Planta* **226**, 647–654 (2007).
17. Lu, K. K. et al. CycC1;1-WRKY75 complex-mediated transcriptional regulation of SOS1 controls salt stress tolerance in Arabidopsis. *Plant Cell* **35**, 2570–2591 (2023).
18. Buendia-Monreal, M. & Gillmor, C. S. Mediator: A key regulator of plant development. *Dev. Biol.* **419**, 7–18 (2016).
19. Kelleher, R. J. 3rd, Flanagan, P. M. & Kornberg, R. D. A novel mediator between activator proteins and the RNA polymerase II transcription apparatus. *Cell* **61**, 1209–1215 (1990).
20. Thompson, C. M., Koleske, A. J., Chao, D. M. & Young, R. A. A multisubunit complex associated with the RNA polymerase II CTD and TATA-binding protein in yeast. *Cell* **73**, 1361–1375 (1993).
21. Kornberg, R. D. Mediator and the mechanism of transcriptional activation. *Trends Biochemical Sci.* **30**, 235–239 (2005).
22. Chong, L., Guo, P. & Zhu, Y. Mediator Complex: A Pivotal Regulator of ABA Signaling Pathway and Abiotic Stress Response in Plants. *Int J. Mol. Sci.* **21**, 7755 (2020).
23. Yang, Y., Li, L. & Qu, L. J. Plant Mediator complex and its critical functions in transcription regulation. *J. Integr. Plant Biol.* **58**, 106–118 (2016).
24. Chong, L., Shi, X. & Zhu, Y. Signal Integration by Cyclin-Dependent Kinase 8 (CDK8) Module and Other Mediator Subunits in Biotic and Abiotic Stress Responses. *Int J. Mol. Sci.* **22**, 354 (2020).
25. Zhu, Y. et al. CYCLIN-DEPENDENT KINASE8 differentially regulates plant immunity to fungal pathogens through kinase-dependent and -independent functions in Arabidopsis. *Plant Cell* **26**, 4149–4170 (2014).
26. Zhu, Y. et al. CDK8 is associated with RAP2.6 and SnRK2.6 and positively modulates abscisic acid signaling and drought response in Arabidopsis. *N. Phytologist* **228**, 1573–1590 (2020).
27. Zhao, J., Favero, D. S., Qiu, J., Roalson, E. H. & Neff, M. M. Insights into the evolution and diversification of the AT-hook Motif Nuclear Localized gene family in land plants. *BMC Plant Biol.* **14**, 266 (2014).
28. Karami, O. et al. An Arabidopsis AT-hook motif nuclear protein mediates somatic embryogenesis and coinciding genome duplication. *Nat. Commun.* **12**, 2508 (2021).
29. Yun, J., Kim, Y. S., Jung, J. H., Seo, P. J. & Park, C. M. The AT-hook motif-containing protein AHL22 regulates flowering initiation by modifying FLOWERING LOCUS T chromatin in Arabidopsis. *J. Biol. Chem.* **287**, 15307–15316 (2012).
30. Favero, D. S. et al. AT-Hook Transcription Factors Restrict Petiole Growth by Antagonizing PIFs. *Curr. Biol.* **30**, 1454–1466 e1456 (2020).
31. Zhang, W. M., Cheng, X. Z., Fang, D. & Cao, J. AT-HOOK MOTIF NUCLEAR LOCALIZED (AHL) proteins of ancient origin radiate new functions. *Int J. Biol. Macromol.* **214**, 290–300 (2022).
32. Rudd, S. et al. Genome-wide in silico mapping of scaffold/matrix attachment regions in Arabidopsis suggests correlation of intragenic scaffold/matrix attachment regions with gene expression. *Plant Physiol.* **135**, 715–722 (2004).
33. Fujimoto, S. et al. Identification of a novel plant MAR DNA binding protein localized on chromosomal surfaces. *Plant Mol. Biol.* **56**, 225–239 (2004).
34. Xu, L. et al. Chromatin attachment to the nuclear matrix represses hypocotyl elongation in Arabidopsis thaliana. *Nat. Commun.* **15**, 1286 (2024).
35. Wong, M. M. et al. Phosphoproteomics of Arabidopsis Highly ABA-Induced1 identifies AT-Hook-Like10 phosphorylation required for stress growth regulation. *Proc. Natl Acad. Sci. USA* **116**, 2354–2363 (2019).
36. Wong, M. M., Huang, X. J., Bau, Y. C. & Verslues, P. E. AT Hook-Like 10 phosphorylation determines ribosomal RNA processing 6-like 1 (RRP6L1) chromatin association and growth suppression during water stress. *Plant Cell Environ.* **47**, 24–37 (2024).
37. Law, J. A. & Jacobsen, S. E. Establishing, maintaining and modifying DNA methylation patterns in plants and animals. *Nat. Rev. Genet.* **11**, 204–220 (2010).
38. Yu, C. W. et al. HISTONE DEACETYLASE6 Acts in Concert with Histone Methyltransferases SUVH4, SUVH5, and SUVH6 to Regulate Transposon Silencing. *Plant Cell* **29**, 1970–1983 (2017).
39. Jing, Y. et al. SUVH2 and SUVH9 Couple Two Essential Steps for Transcriptional Gene Silencing in Arabidopsis. *Mol. Plant* **9**, 1156–1167 (2016).
40. Liu, Z. W. et al. The SET domain proteins SUVH2 and SUVH9 are required for Pol V occupancy at RNA-directed DNA methylation loci. *PLoS Genet.* **10**, e1003948 (2014).
41. Jiang, H. et al. Ectopic application of the repressive histone modification H3K9me2 establishes post-zygotic reproductive isolation in Arabidopsis thaliana. *Genes Dev.* **31**, 1272–1287 (2017).
42. Kuhlmann, M. & Mette, M. F. Developmentally non-redundant SET domain proteins SUVH2 and SUVH9 are required for transcriptional gene silencing in Arabidopsis thaliana. *Plant Mol. Biol.* **79**, 623–633 (2012).
43. Naumann, K. et al. Pivotal role of AtSUVH2 in heterochromatic histone methylation and gene silencing in Arabidopsis. *Embo J.* **24**, 1418–1429 (2005).
44. Hsu, C. C. et al. Universal Plant Phosphoproteomics Workflow and Its Application to Tomato Signaling in Response to Cold Stress. *Mol. Cell Proteom.* **17**, 2068–2080 (2018).
45. Wang, P. et al. Mapping proteome-wide targets of protein kinases in plant stress responses. *Proc. Natl Acad. Sci. USA* **117**, 3270–3280 (2020).
46. Hollomon, J. M. et al. The Candida albicans Cdk8-dependent phosphoproteome reveals repression of hyphal growth through a Flo8-dependent pathway. *PLoS Genet.* **18**, e1009622 (2022).
47. Poss, Z. C. et al. Identification of Mediator Kinase Substrates in Human Cells using Cortistatin A and Quantitative Phosphoproteomics. *Cell Rep.* **15**, 436–450 (2016).
48. Dong, J. et al. An R2R3-MYB Transcription Factor RmMYB108 Responds to Chilling Stress of Rosa multiflora and Conferred Cold Tolerance of Arabidopsis. *Front Plant Sci.* **12**, 696919 (2021).
49. Ding, Z. et al. Transgenic expression of MYB15 confers enhanced sensitivity to abscisic acid and improved drought tolerance in Arabidopsis thaliana. *J. Genet Genomics* **36**, 17–29 (2009).
50. Jiang, Y., Yang, B. & Deyholos, M. K. Functional characterization of the Arabidopsis bHLH92 transcription factor in abiotic stress. *Mol. Genet. Genomics: MGG* **282**, 503–516 (2009).
51. Wu, A. et al. JUNGBRUNNEN1, a reactive oxygen species-responsive NAC transcription factor, regulates longevity in Arabidopsis. *Plant Cell* **24**, 482–506 (2012).

52. Aravind, L. Landsman D. AT-hook motifs identified in a wide variety of DNA-binding proteins. *Nucleic Acids Res.* **26**, 4413–4421 (1998).
53. Lin, H. et al. Phosphorylation of SOS3-LIKE CALCIUM BINDING PROTEIN8 by SOS2 protein kinase stabilizes their protein complex and regulates salt tolerance in Arabidopsis. *Plant Cell* **21**, 1607–1619 (2009).
54. Quan, R. et al. SCABP8/CBL10, a putative calcium sensor, interacts with the protein kinase SOS2 to protect Arabidopsis shoots from salt stress. *Plant Cell* **19**, 1415–1431 (2007).
55. Rayapuram, N. et al. Chromatin phosphoproteomics unravels a function for AT-hook motif nuclear localized protein AHL13 in PAMP-triggered immunity. *Proc. Natl Acad. Sci. USA* **118**, e2004670118 (2021).
56. Xiao, C., Chen, F., Yu, X., Lin, C. & Fu, Y. F. Over-expression of an AT-hook gene, AHL22, delays flowering and inhibits the elongation of the hypocotyl in Arabidopsis thaliana. *Plant Mol. Biol.* **71**, 39–50 (2009).
57. Zhao, J., Favero, D. S., Peng, H. & Neff, M. M. Arabidopsis thaliana AHL family modulates hypocotyl growth redundantly by interacting with each other via the PPC/DUF296 domain. *Proc. Natl Acad. Sci. USA* **110**, E4688–E4697 (2013).
58. Zhang, S. et al. Widely conserved AHL transcription factors are essential for NCR gene expression and nodule development in Medicago. *Nat. Plants* **9**, 280–288 (2023).
59. Walton, R. T., Christie, K. A., Whittaker, M. N. & Kleinstiver, B. P. Unconstrained genome targeting with near-PAMless engineered CRISPR-Cas9 variants. *Sci. (N. Y., NY)* **368**, 290–296 (2020).
60. Guo, P. et al. Genome-wide survey and expression analyses of the GRAS gene family in *Brassica napus* reveals their roles in root development and stress response. *Planta* **250**, 1051–1072 (2019).
61. Sang, T. et al. DIA-Based Phosphoproteomics Identifies Early Phosphorylation Events in Response to EGTA and Mannitol in Arabidopsis. *Mol. Cell. Proteom.* **23**, 100804 (2024).
62. Guo, P. et al. Mediator tail module subunits MED16 and MED25 differentially regulate abscisic acid signaling in Arabidopsis. *J. Integr. Plant Biol.* **63**, 802–815 (2021).
63. Chong, L. et al. The tomato OST1-VOZ1 module regulates drought-mediated flowering. *Plant Cell* **34**, 2001–2018 (2022).
64. Zhu, Y. et al. Analysis of interactions among the CLAVATA3 receptors reveals a direct interaction between CLAVATA2 and CORYNE in Arabidopsis. *Plant J.: Cell Mol. Biol.* **61**, 223–233 (2010).
65. Chen, C. et al. TBtools-II: A “one for all, all for one” bioinformatics platform for biological big-data mining. *Mol. Plant* **16**, 1733–1742 (2023).
66. Zhu, Y. et al. A natural promoter variation of SlBBX31 confers enhanced cold tolerance during tomato domestication. *Plant Biotechnol. J.* **21**, 1033–1043 (2023).
67. Allen, J. J. et al. A semisynthetic epitope for kinase substrates. *Nat. Methods* **4**, 511–516 (2007).
68. Lim, P. O. et al. Overexpression of a chromatin architecture-controlling AT-hook protein extends leaf longevity and increases the post-harvest storage life of plants. *Plant J.: Cell Mol. Biology* **52**, 1140–1153 (2007).
69. Saleh, A., Alvarez-Venegas, R. & Avramova, Z. An efficient chromatin immunoprecipitation (ChIP) protocol for studying histone modifications in Arabidopsis plants. *Nat. Protoc.* **3**, 1018–1025 (2008).
70. Zhu, J. Y., Sun, Y. & Wang, Z. Y. Genome-wide identification of transcription factor-binding sites in plants using chromatin

immunoprecipitation followed by microarray (ChIP-chip) or sequencing (ChIP-seq). *Methods Mol. Biol.* **876**, 173–188 (2012).

Acknowledgements

We would like to thank Prof. Pengcheng Wang and Dr. Tian Sang (Southern University of Science and Technology) as well as Dr. Chuan-Chih Hsu and Prof. Andy Tao (Purdue University) for their help on phosphoproteomics analysis. This work was supported by the National Natural Science Foundation of China (NSFC) grants 32350610245, 32270308, and by the Technological Innovation Talents in Colleges and Universities in Henan, China (23HASTIT036).

Author contributions

Y.Z. conceived and designed this project. P.G. and L.C. performed most experiments, R.X. and Z.J. conducted ChIP-qPCR and some molecular experiments. Q.N. performed ChIP-seq experiments and data analysis. P.G., R.X. and L.C. analyzed the data and provided valuable comments. P.G., L.C. and Y.Z. wrote and revised the manuscript.

Competing interests

The authors declare no competing interests.

Additional information

Supplementary information The online version contains supplementary material available at <https://doi.org/10.1038/s41467-025-57806-6>.

Correspondence and requests for materials should be addressed to Yingfang Zhu.

Peer review information *Nature Communications* thanks the anonymous reviewers for their contribution to the peer review of this work. A peer review file is available.

Reprints and permissions information is available at <http://www.nature.com/reprints>

Publisher's note Springer Nature remains neutral with regard to jurisdictional claims in published maps and institutional affiliations.

Open Access This article is licensed under a Creative Commons Attribution-NonCommercial-NoDerivatives 4.0 International License, which permits any non-commercial use, sharing, distribution and reproduction in any medium or format, as long as you give appropriate credit to the original author(s) and the source, provide a link to the Creative Commons licence, and indicate if you modified the licensed material. You do not have permission under this licence to share adapted material derived from this article or parts of it. The images or other third party material in this article are included in the article's Creative Commons licence, unless indicated otherwise in a credit line to the material. If material is not included in the article's Creative Commons licence and your intended use is not permitted by statutory regulation or exceeds the permitted use, you will need to obtain permission directly from the copyright holder. To view a copy of this licence, visit <http://creativecommons.org/licenses/by-nc-nd/4.0/>.

© The Author(s) 2025